FINITE ELEMENT SIMULATION OF INTRA-PELLET ADSORPTION AND HEAT TRANSFER

DADA, AKINDOLU OLUWAKANYINSOLA

A dissertation submitted to the University of Bristol in accordance with the requirements of the degree of Master of Scienceby advanced study in Mechanical Engineering in the Faculty of Engineering

Department of Mechanical Engineering

September 2011

15,157 words

ABSTRACT

Adsorption chillers have been proposed as a means of generating low cost cooling, but the coefficient of performance of these machines are quite low and this has hindered their use in practical applications. Due to this problem the adsorption process has generated much research interest.

Research carried out on the adsorption process has shown that the loading capacity of a pellet affects the rate of adsorption and consequently the COP of machines based on these adsorbents. It has also been shown that temperature affect the loading capacity of an adsorbent and consequently the COP of adsorption chillers.

In this research the effect of temperature on the rate of adsorption was investigated. This was done by creating finite elements models of the adsorption process. These models coupled the heat and mass transfer processes that occur during adsorption. The first two models created were the conventional LDF model, which has been used extensively to model the adsorption process because of its linear nature and ease of use. The third model created was the diffusion model. The diffusion model was created in a bid to detect salient features of the adsorption model which the LDF model might not be able to detect. The models were then verified by comparing with experimental work carried out by Ahamat and Tierney[1]

The verified models were used in carrying out several simulations in which different parameters of the adsorbent or the adsorption process was varied.

It was observed that the LDF model and the diffusion model gave somewhat different results when used to simulate the same process, and this was observed to be due to the fact that the LDF model assumes a mean loading for the entire domain and does not take into account the spatial temperature gradients occurring over the domain.

It was also observed that, contrary to what was generally believed that an increase in temperature ultimately leads to a reduction in the rate of adsorption. The diffusion model showed a different trend. From the diffusion model, it was observed that increase in temperature could have different effects depending on when and where this temperature change occurs. Temporary increase in temperature at the start of adsorption occurs near the edge of the pellet and brings about an increase in the rate of adsorption. While on the other hand a temporary decrease in temperature at the start of adsorption that occurs at the edge of the pellet results in a reduction in the rate of adsorption.

DEDICATION

This work is dedicated to the glory of God and the memory of my grandmother Emily Ajibabi Doherty (1917 - 2005)

ACKNOWLEDGEMENTS

I would like to appreciate the efforts of individuals and organisations that contributed to the success of this work in one way or another.

Firstly I want to appreciate the effort of my supervisor, Dr. Mike Tierney for his mentorship, advice and encouragement, and also for providing his Axisymmetric routines freely to be used in the research work. Your effort is highly appreciated and would never be forgotten.

Secondly I want to acknowledge the immense financial support provided by the Petroleum Technology Development Fund (PTDF) of the Federal Republic of Nigeria, on whose sponsorship I am studying in the University of Bristol. None of these would have been possible without their funding. God bless PTDF and God bless the Federal Republic of Nigeria.

I would also like to appreciate the efforts of all others that contributed to the success of this work, Mohamad Asmidzam Ahamat for granting access to results of your experimental work and for invaluable discussion, Fan Yin for invaluable discussion, Avi Banerjee for discussions on style and initial proof readings.

Finally I would like to appreciate the input of all friends and colleagues who were of immense value during my programme here, the list is too long to fit in here but your names and contributions are boldly written in my heart and would never be forgotten.

AUTHOR'S DECLARATION

I declare that this work was carried out in accordance with the requirements of the University's Regulations and Code of Practice for Taught Postgraduate Programmes and that it has not been submitted for any other academic award. Except where indicated by specific reference in the text, this work is my own work. Work done in collaboration with, or with the assistance of others, is indicated as such. I have identified all material in this dissertation which is not my own work through appropriate referencing and acknowledgement. Where I have quoted from the work of others, I have included the source in the references/bibliography. Any views expressed in the literature are those of the author.

SIGNED: …… DATE: ……..

(Signature of student/candidate)

NOMENCLATURE

Upper Case Letters

AXI	Axisymmetric
C	Concentration (kg/m^3)
CART	Cartesian
COP	Coefficient of Performance
D	Diffusivity (m^2/sec)
D_{so}	Surface diffusivity at zero loading
E_a	Activation energy (J/mol)
FD	Fickian Diffusion
K	Henry's constant (1/Pa)
K_{ldf}	Linear Driving Force constant (1/sec)
K_o	Pre-exponent factor (1/Pa)
LDF	Linear Driving Force
P	Pressure (pa)
Q	Heat of adsorption (J/kg)
R_g	Gas constant (J/kgK)
R_m	Molar gas constant (J/molK)
T	Temperature (K)
X	Loading (kg/kg)
X*	Equilibrium loading (kg/kg)
W_o	Monolayer adsorption capacity

Lower Case Letters

c_p	Specific heat capacity (J/kgK)
k	Thermal conductivity (W/mK)
n	Normal direction to surface
$\dot{q}$	Volumetric heat generation (W/m^3)
r	radius (m)
t	time (sec)
t'	Toth parameter
x	x direction in the Cartesian coordinate
y	y direction in the Cartesian coordinate

Greek Letters

∂	Partial derivative
ε	Porosity
∇	Gradient of a scalar field
ρ	Density (kg/m^3)

Subscripts

ads	adsorber
app	Apparent
evap	evaporator
fin	fin or heat transfer surface
ldf	Linear Driving Force
s	Surface

Superscripts

pore	Pore
surf	Surface

TABLE OF CONTENTS

LIST OF TABLES

LIST OF FIGURES

CHAPTER 1 INTRODUCTION

1.1 Introduction

Due to increasing cost of energy, environmental concerns, and the relatively large energy requirements of refrigeration systems[2-5], better alternatives to the existing systems are being sought. A promising alternative is the adsorption chiller.

Adsorption chillers have generated much research interest because of their potential of providing low cost cooling; this is mainly due to the counter-intuitive approach of using heat to generate cooling and the ability of these systems to make use of waste heat or solar heat. These energy sources are usually available at little or no cost, the major cost involved is that of providing the equipment required to harvest the energy.

Despite the research interest and the depth and breadth of research carried out in this area, the coefficient of performance (COP) of these systems is not as good as that of the conventional vapour compression system[6]. The COP of a refrigeration system has a direct effect on its capital cost, as lower COP implies that a larger refrigeration system would be required to provide the same cooling capacity that a smaller system with a higher COP would provide.

Application of adsorption in the fields of chemistry for purification of gases and for chromatography considers the mass transfer process, and little attention is given to the heat transfer process and the effects of temperature. For these processes the ultimate goal is removal of a given quantity of material from a mixture, or separation of the components of a mixture of gases or liquids. Whereas in the case of the application of adsorption in refrigeration the mass transfer as well as the heat transfer process is relatively important. In the case of separation if more material has to be removed, the size of the bed is increased and this effect is obtained, but for refrigeration the important factor is the rate of adsorption per unit mass, a larger bed might not offer much improvement in performance, because an increase in the size of the bed also results in greater heat transfer surface for heat gains and heat loss. Therefore the most important thing in the application of adsorption to refrigeration system is to improve the heat removal rate (or adsorption rate) per unit mass of adsorbent.

To achieve this improvement in performance it is important that, we have a means of studying the adsorption process in detail, to fully understand the kinetics of the process. If possible models should be created that would be able to simulate the process to the molecular level, in order to get an insight into the connection between the heat and mass transfer processes occurring in it. By doing this we would be able to design better systems that make use of the optimal characteristics of the system and eliminate unnecessary heat losses and gains from the system.

The adsorption process is usually accompanied by heat gains, as heat of adsorption. This heat gain is similar to the latent heat of vaporization, and this causes the temperature in the pellet to increase as the adsorption process progresses. Temperature increase has been shown to have two opposing effect on the rate of adsorption. The loading capacity of an adsorbent is inversely proportional to the temperature of the adsorbent, whereas the diffusivity is directly proportional to the temperature. These two effects affect the rate of adsorption and consequently the performance of the system.

A method proposed by Ahamat and Tierney [1]suggests bonding the pellet directly to a heat transfer surface, as opposed to packing it in a bed. This configuration has the potential of increasing the rate of heat transfer to and from the pellet. This configuration was investigated in this research in order to determine how hot the pellet gets and also to determine the effect of temperature on adsorption.

Experiments were not carried out due to the financial implication, similar experiments have already been done by [1], and experiments cannot see inside the pellet, and this is what we intend to do.

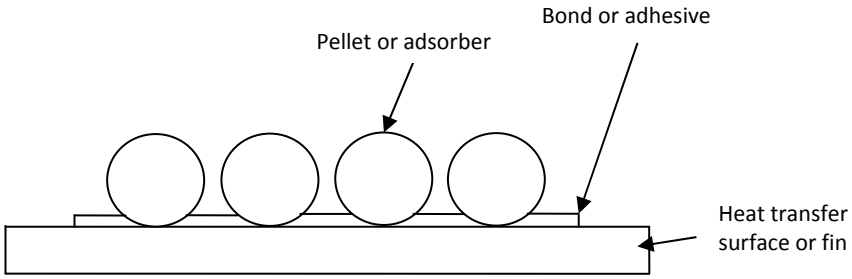

Figure 1.1 Adsorber bonded to heat transfer surface

In this research work, the effect of temperature on the adsorption process was investigated, and then by means of deduction, the effect of diffusivity and loading capacity on the rate of adsorption was determined. In order to do this, three models were created to simulate the adsorption process. These were created using the linear driving force (LDF) and Fickian diffusion (FD) for the mass transfer part of the process, the first two models were based on the LDF while the last one was based on FD. The heat and mass transfer processes were coupled. The heat transfer in both models is the same while the mass transfer is what distinguishes between the LDF and FD models. Having such models would enable the adsorption process to be simulated and studied for salient features which may not be observable in physical experiment. After creating the models, a verification stage was carried out . In the verification stage simulations which replicate physical experiments were carried out, and the results obtained from the simulation were compared with those from the experiment. It was observed that the results from the simulation was in close approximation to those of the experiment. After the models were verified, the model was then used in simulating different experiments, the results of which are discussed in the fifth chapter of this report.

CHAPTER 2 LITERATURE REVIEW

This chapter reviews some basic concepts of adsorption and also previous research done in the area of adsorption refrigeration, adsorbents, working pairs, adsorption modeling, and mass transfer in adsorbents

2.1 Historical Development of Adsorption and Adsorption Chillers.

"Adsorption cycles for refrigeration were first used in the early 1900s as reported by Plank and Kuprianoff. Machines using both the adsorbent-refrigerant pairs CaCl2 - NH3 and carbon-methanol were successfully manufactured." [7]. The development of the hermitic compressor and the Platen-Munters absorption cycle led to the demise of these early systems[7], and according to Wang and Oliveira[8] renewed interest in solid sorption refrigeration started around the 1970s due to the energy crisis and then later in the 1990s because of ecological problems (ozone depletion and greenhouse effect) related to the use of CFCs and HCFCs as refrigerants.

2.2 Isotherms

The adsorption process has been studied extensively by various researchers, and from their studies, different isotherms of adsorption were derived, some of which are; Langmuir isotherm , Fruedlinch isotherm, Toth isotherm, Henry's isotherm, Dubinin Ashtakov isotherm, and Braenuer Emmett Teller (BET) isotherm.

The different isotherms apply to the adsorption process in different adsorbent-adsorbate pairs. The isotherms model the adsorption of an adsorbate into an adsorbent at constant temperature, where the quantity adsorbed is given as a function of pressure. The first five isotherms mentioned above apply to monolayer adsorption, while the last one (BET Isotherm) applies to multilayer adsorption. Generally there are five types of adsorption isotherms [9], the different isotherms mentioned above are all classified into one of the five types of isotherms shown in Figure 2.1 below. The adsorption process in an adsorbent-adsorbate pair is normally modeled by one of these isotherm types.

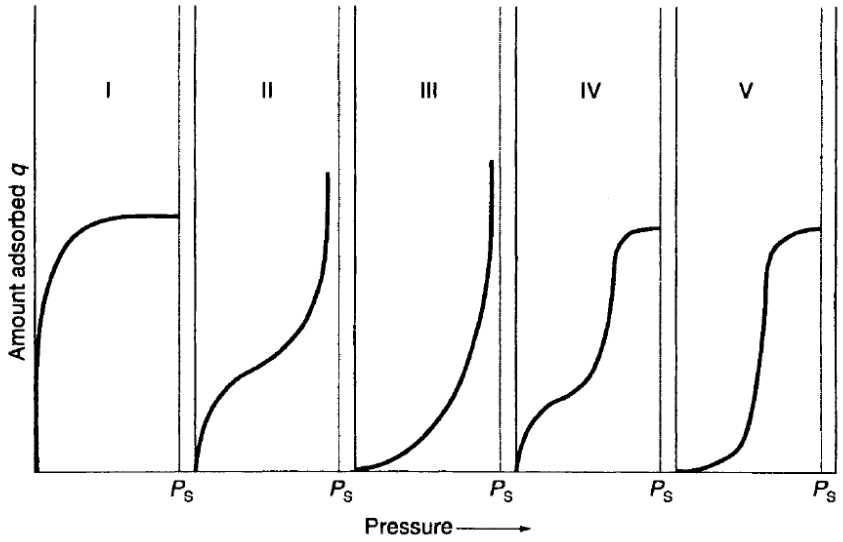

Figure 2.1 Different isotherm types; Thomas and Crittenden[9]

According to Do [10] the type I isotherm is observed for adsorption of gases on microporous solids whose pore sizes are not much larger than the molecular diameter of the adsorbate, therefore complete filling of these narrow pores corresponds to the completion of a molecular monolayer. Microporous adsorbents are used extensively in refrigeration, therefore the type I isotherm is of main concern. Yang [11], Thomas and Crittenden [9], Suzuki [12] and Do [10] discuss the other isotherm types in detail.

This research would be studying adsorption in microporous silica gel, therefore the type I isotherm would be used. For the models created the Toth's Isotherm was employed. The Toth equation is given in equation 3.10

2.3 Adsorbents

There are different types of adsorbents which are employed in adsorption, and for each adsorbent there is a suitable adsrobate (or suitable adsorbates) with which it can be used. The main determining factor of in selecting a suitable adsorbate for an adsorbent is the polarity. Therefore adsorbent-adsorbate pairs are normally grouped into polar and non-polar. a more detailed discussion on the different adsorbent-adsorbate pairs is given in the section on working pairs.

Yang [11], carried out a detailed analysis of different adsorbents, and he discusses how they are manufactured, their chemical composition, porosity, and he also carried out a detailed analysis of their adsorption kinetics. Srivastava [13] also considered various adsorbent-adsorbate working pairs and their characteristics with respect to solid-vapour heat pumps.

The adsorbent-adsorbate working pair which would be modeled in this research is the silica gel-water pair. This was chosen because of the existence of experimental data with which the simulation results can be compared. Some benefits of this working pair is that It is cheaper and non-toxic and also has a high loading capacity.

2.3.1 Silica Gel and Its Characteristics

Silica gel is a common substance often used as a desiccant, this is due to its affinity to adsorb water and it's large water adsorbing capacity (RD silica gel being able to adsorb about 40% by weight) coupled with its low cost. It is normally found in electronic components, where it is included to adsorb moisture from the package and prevent the components from corrosion due to moisture.

Due to the properties mentioned above silica gel is a suitable adsorbent for adsorption refrigerators employing water as the refrigerant. Another property of silica gel that makes it a desirable candidate adsorbent for adsorption refrigeration is its ease of regeneration; requiring about 150^{o}C for regeneration after adsorption, therefore making it suitable for various low-grade heat sources, such as solar, and waste heat.

According to Yang [11]Silica gel can be formed by two routes:

- Polymerization of silicic acid: Silicic acid, $Si(OH)_4$ polymerizes easily to form a network of siloxane (Si-O-Si), leaving a small number of uncondensed Si-O-H groups.
- Aggregation of particles of colloidal silica: this involves the coagulation of silica sols of almost equal sizes. These sub-micrometer particles can coagulate by van der Waals forces or by cations bridging as coagulants.

Commercial silica gel is usually produced via the first route[11], and has pore size in the range of 6-25nm and surface areas in the range of 100-850m^2/g, depending on whether the gel is low density or regular density[9].

Regular density gel has a surface area of 750-850 m^2/g and an average pore diameter of 2.2-2.6 nm, while low density silica gel has a surface area of 300-350 m^2/g and pore diameter of 100-150nm.

The pore size distribution of silica gel is shown in the Figure 2.2 below,

Adsorption of water and other substance to silica gel occurs mostly by the formation of hydrogen bonds between the adsorbate molecules and the silanol groups (SiOH). [11]

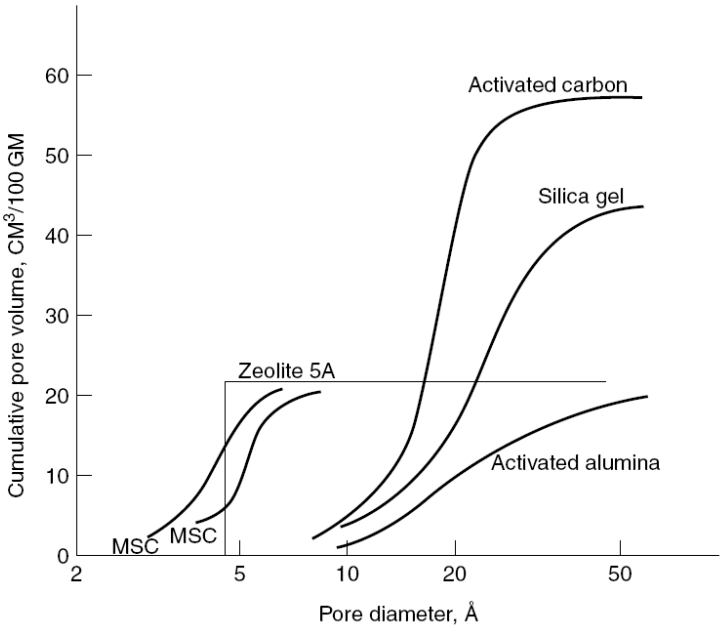

Figure 2.2 .Pore-size distribution for activated carbon, silica gel, activated alumina, two molecular sieve carbons, and zeolite 5A, [11]

2.4 Working Pairs

Working pairs for the adsorption process are usually classified based on two criteria, the first being the type of adsorption that takes place and the second being the polarity of the adsorbent.

Based on the first criteria, working pairs could be classified as either physical or chemical; in the former the adsorption process takes place by a physical means, while the latter involves a chemical reaction in which chemical bonds are formed or broken.

The other criteria is the polarity, and working pairs are classified as either polar or non-polar based on this criteria. In polar working pairs, both the adsorbate and the adsorbent are polar, the same obtains for the non-polar working pairs. Working pairs are mostly classified based on this criteria, Srivastava and Eames[13] gave a list of commercial hydrophilic(Polar) solid sorbents and commercial hydrophobic(non-polar) solid sorbents. Most hydrophobic solid sorbents can be used with a range of hydrophobic sorbates, and the same goes for the hydrophillic sorbents also, they can also be used with a range of hydrophilic sorbates. The performance of the sorbate-sorbent combination usually determines which option is mostly employed commercially.

According to Srivastava and Eames[13] some commercial Hydrophilic Solid Sorbents are; Silica gel, Activated (or porous) Alumina, Zeolites, and Calcium Cholride. While commercial Hydrophobic Solid Sorbents are; Activated Carbons, Metal Oxides, specially developed porous metal hydrides, and composite adsorbents.

Wang et.al[14] reviewed various working pairs used in adsorption refrigeration, and came out with the performance analysis shown in Table 2.1 below.

Evaporating Temperature (^{o}C)	Adsorption working pair	COP	SCP (W/kg)	Characteristics
8	Activated carbon/NH_3		1000	Convective thermal wave cycle
1	Activated carbon fibre/$CaCl_2$/NH_3	0.6	330	Composite adsorbent, heat pipe heating
3	Activated carbon/NH_3	0.67	557	Convective thermal wave cycle
-10	$SrCl_2$-NH_3	0.32	230	Single effect system
-25	($MnCl_2$ + $NiCl_2$) - NH_3	0.4	70 x 2	Double effect system
-10	Metal hydride/Hydrogen	0.43	25 x 2	Thermal wave cycle
3	Graphite/Silica gel/Water		35 x 2	Composite adsorbent to intensify the heat transfer
10	Silica gel/Water	0.4	85	Split heat pipe type evaporator
5	Zeolite/Water	0.9	125 x 2	Intermittent convective thermal wave cycle
-15	$CaCl_2$/Activated carbon/Ammonia	0.41	731	Composite adsorbent, heat pipe type heating and cooling
-25	$CaCl_2$/Activated carbon/Ammonia	0.36	627.7	Composite adsorbent, heat pipe type heating and cooling
-15	$CaCl_2$/Graphite/Ammonia	0.3	1000	Composite adsorbent

Table 2.1 Review of working pairs used in adsorption chillers Wang et.al[14] (Permission requested)

According to Wang et.al [14], the silica gel-water working pair is one of the most studied physical adsorption working pairs, and some of the reasons for this is because of its low desorption temperature which makes it suitable for solar energy utilization. However it is impossible to produce evaporator temperatures below 0^{o}C with this working pair, thereby limiting its use to chillers.

2.5 Adhesive / Bond

Heat transfer between the silica gel and the fin occurs mainly through the adhesive. It is therefore important to use an adhesive material with good adhesion properties so as to ensure good contact with the silica gel and the metal surface of the fin, as this minimizes the contact resistance by excluding air gaps from the contact surface. An adhesive with high thermal conductivity should also be chosen so as to maximize the heat transfer from the silica gel to the fin.

The thermal conductivity of the adhesive, the thermal resistance of the silica gel-adhesive bond, and that of the adhesive-metal bond can be lumped into a single thermal resistance (or contact resistance) between the silica gel and the fin.

A suitable adhesive would be one which minimizes this lumped thermal resistance.

Several adhesive types have been used in bonding silica gel to a fin or heat transfer surface. Some of these are "epoxy resin [15], RS 'super' thermal paste [16] and Artic silver [17]

2.6 Adsorption Modeling

Models give us the ability to study a system without setting up expensive and time consuming experiments. If an accurate model is created, it gives the possibility of carrying out virtual experiments which do not have the shortcomings of physical experiments, shortcomings like scale, measurement noise, inaccuracies of sensors, time, and the inability to set up a perfect control experiment etc.

Modeling of the adsorption process has generated much interest for some of the following reasons, a mathematical model gives us the ability to simulate the adsorption process and then observe the effect of several factors on it. It also enables us to scale down the virtual experiment to that of a single pellet and examine what happens during adsorption in a single pellet; something which is quite difficult with real experiments because of the small size of the pellet.

Most adsorption models that have been created are for a bed of silica gel, [18-22] carried out studies on the adsorption process and created models while doing this. The first four researches modeled an adsorbent bed, while the last one modeled adsorption in a single pellet. Of all the studies carried out on adsorption in which models were created only a few ones actually model the adsorption process for a single pellet. This might be attributable to difficulty involved in carrying out experiments for a single pellet so the result from the model can be compared to (and verified by) that of the experiment.

However it is necessary that we properly understand the adsorption process that goes on in a single pellet of silica gel as this would enable the design of adsorption chillers using a bottom-up approach. This approach could be used to design optimal adsorbent beds based on the adsorption characteristics of the pellet, and in turn the entire chiller is design based on the characteristics of the bed.

2.7 Intraparticle Diffusion

The mass diffusion process into adsorbents has been studied by various researchers, but of all these, the one of interest here is the adsorption into silica gel. Most of the research carried out on adsorption into silica gel was done on a bed of silica gel, as the silica gel pellet is quite small and it is difficult to carry out detailed experimental investigation on it.

Adsorption into adsorbents can either be modeled using the Linear Driving Force (LDF) model (Glueckauf [23]) or the diffusion model. The linear driving force model has been studied by several researchers [24], [19], [20], [18]. The LDF model has been taken to be a good approximation for the diffusion process that takes place in adsorbents, and this method has been considered to be reasonably accurate. The LDF model is mainly used because it is linear and easy to use, it is derived by setting the storage $\left(\frac{\partial X}{\partial t}\right)$ term in Fick's second law as constant throughout the pellet domain[25]. Recent research now shows that the LDF model does not always give an accurate approximation of the diffusion process.

El-Sharkawy [19], compared the classical LDF model with the Fickian Diffusion (FD) model. He observed that the LDF model had numerous errors at relatively short adsorption times and inferred that these errors may result in incorrect evaluation of adsorption chiller performance, especially at short cycle times. He also proposed a modified form of the LDF model which tries to reduce these errors by considering the effect of the particle mass transfer coefficient on the dimensionless time.

From the results obtained by El-Sharkawy [19], it can be observed that; when the LDF model is used there is a significant under-prediction of the adsorption at short adsorption times.

Raymond and Garimella [20] also carried out a similar study in which they compared the LDF model with the FD model, and observed errors in the LDF model. The result obtained by Raymond and Garimella also showed that the LDF model under-predicts the adsorption at short adsorption times, and over predicts it at longer adsorption times. Raymond and Garimella also considered the effect of various conditions on the error between the LDF and the FD model and they found out that a step change in the surface adsorbate content for an isothermal particle is the boundary condition that yields the maximum LDF error. They then concluded that this provides a conservative bound for the LDF error under non-isothermal conditions.

One of the main problems normally encountered in modeling the diffusion process is that of accurately predicting the diffusivity of the adsorbent. For one the diffusivity is difficult to measure for a single pellet, so most experiments evaluate the diffusivity of a bed and adjust the obtained value to get that of a single pellet. Even when this is obtained the diffusivity of silica gel varies from batch to batch, so the diffusivity of a particular batch may be significantly different from that for another batch. As a result most models should be supported by experimental data for the current batch of silica gels.

As a result of the above problem it is quite difficult to produce a model that would fit all adsorption processes regardless of the batch of silica gel. Any generalized model would at its best be a rough approximation of the adsorption process; and this is what the LDF model does, it gives a generalized rough approximation of the adsorption process.

From the studies carried out by [19] and [20] they hinted about the presence of errors in the LDF model at short adsorption times, these results seem realistic and the result from the two researches corroborated each other. Though these results were not compared with experimental data, it demonstrated that there could be noticeable differences between the predicted adsorption obtained from an LDF model and the FD model.

2.8 Pore / Surface Diffusion Model

There are generally two methods of creating a FD model; it can either be modeled as surface or pore diffusion. The choice of which model to be used depends on the properties of the adsorbate, adsorbent and also the adsorption condition.

The FD model usually described mathematically by Fick's second law of diffusion equation(2.1) Requires a diffusivity term, this term is what contains the surface or pore diffusivity term.

$$\frac{\partial C}{\partial t} = \frac{D_{app}{}_{app}^{pore}}{r^2}\frac{\partial}{\partial r}\left(r^2\frac{\partial C}{\partial r}\right) \qquad (2.1)$$

Based on work carried out by Pesaran and Mills[26, 27] it was observed that intra-particle moisture transport in micro porous silica gel is dominated by surface diffusion while for macro porous silica gel both Knudsen and surface diffusion is important. According to [20] when surface diffusion dominates (as in micro porous silica gel) and the value of the Henry's constant is large, then the apparent diffusivity value can be approximated to that of the surface diffusivity (D_s).

$$D_{app}{}_{app}^{surf} \approx D_s \qquad (2.2)$$

2.9 Thermal Conductivity

The thermal conductivity of silca gel has been shown to vary during the adsorption process, and the variation has been shown to be related to the loading of the pellet. Gurgel and Kluppel [28] measured the thermal conductivity of hydrated silica gel and they observed that the thermal conductivity of the solid silica gel varies with the loading of the pellet, from their experiment they observed that the thermal conductivity of the solid silica gel varied between 0.7W/mK to about 1.2W/mK, and the variation was linear. Tanashev and Aristov [29] also observed a relationship between thermal conductivity and loading of the silica gel pellet.

Carson et.al [30] studied the influence of material structure on the effective thermal conductivity of theoretical porous materials using finite element simulations. From this study it was observed that the effective thermal conductivity of the material increased with the increase in inclusion if the thermal conductivity of the inclusion was higher than the continuous phase and vice-versa. This justifies the result obtained by [28] and [29] as increase in loading results in the air-filled pores of the silica gel pellet being replaced by water which is of a higher thermal conductivity, therefore an increase in effective thermal conductivity is expected, which is what was measured in the experiment by [28] and [29].

2.10 Adsorption Cycle

A typical adsorption cycle is represented by the cycle diagram shown in Figure 2.3, the cycle consists of the following processes:

- 1-2 Isosteric heating: the adsorber is heated and pressurized until desorption of the sorbate starts, this heating stage takes place at constant adsorber loading.
- 2-3 Heating and Desorption: the adsorber is heated at constant pressure to make it desorb some or all of the sorbate. In this stage the adsorber is connected to the condenser and the desorbed sorbate flows into the condenser where it is cooled and allowed to condense
- 3-4 Isosteric cooling: the adsorber is cooled down and depressurized after desorption, this cooling stage takes place at constant adsorber loading.
- 4-1 Cooling and Adsorption: the adsorber is cooled and connected to the evaporator, the sorbate flows from the evaporator to the adsorber where it is adsorbed. This stage takes place at a constant pressure which is the evaporator pressure.

And two other processes which occur outside the adsorbent bed, these are:

- 6-1 Evaporation: As the sorbate evaporates from the evaporator it gains the heat of vaporization from the evaporator, therefore creating a cooling effect in the evaporator, the sorbate vapour then flows to the adsorber where it is then adsorbed.
- 2-3 Condensation: As the desorbed sorbate flows from the adsorber to the condenser it is condensed, and then allowed to flow back to the evaporator, ready for the next cycle.

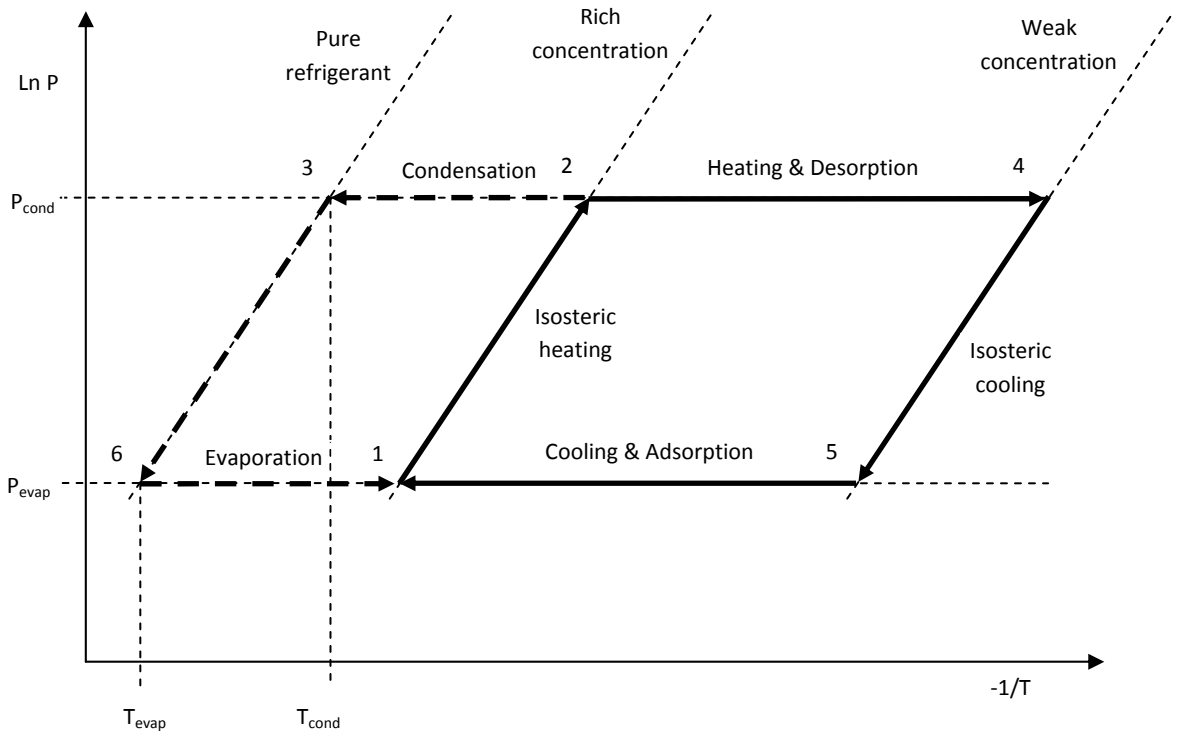

Figure 2.3 The adsorption cycle; depicted by the Clapeyron diagram

The work reported models the adsorption process, in which the internal heat generation in the process is a direct result of the rate of adsorption (or rate of change in concentration of adsorbate in the adsorbent). The rate of adsorption is also affected by the temperature of adsorbent, which is dependent on the internal heat generation term. Therefore it can be said that the adsorption process is a coupled heat and mass transfer process.

CHAPTER 3 THEORY ON THE ADSORPTION PROCESS

This section discusses the theoretical formulation of the adsorption problem, and also gives the necessary equations required to model the process. These equations are then used in building the model in Chapter 4.

The heat transfer is discussed first, followed by the mass transfer, these two are then coupled.

3.1 Heat Transfer

Heat transfer in the pellet is modeled by the heat conduction equation with the appropriate boundary conditions applied to it. The general heat conduction equation is given as

$$\rho c_p \frac{\partial T}{\partial t} = \nabla.(k\nabla T) + \dot{q} \qquad (3.1)$$

where k is the thermal conductivity, ρ is the density, c_p is the heat capacity, and q̇ is the internal heat generation. We would assume k to be constant throughout the entire domain, therefore the heat conduction equation reduces to the form shown below.

$$or \;\; \rho c_p \frac{\partial T}{\partial t} = k\nabla^2 T + \dot{q} \quad when\ k = constant$$

3.1.1 Cartesian Formulation

In Cartesian coordinates

$$\nabla^2 T = \frac{\partial^2 T}{\partial x^2} + \frac{\partial^2 T}{\partial y^2} + \frac{\partial^2 T}{\partial z^2}$$

The problem can be reduced to 2 dimensions where $\frac{\partial^2 T}{\partial z^2} = \frac{\partial T}{\partial z} = 0$ therefore $\nabla^2 T$ reduces to:

$$\nabla^2 T = \frac{\partial^2 T}{\partial x^2} + \frac{\partial^2 T}{\partial y^2} \qquad (3.2)$$

The conduction equation for the Cartesian pellet problem with constant thermal conductivity is given below:

$$\rho c_p \frac{\partial T}{\partial t} = k\left(\frac{\partial^2 T}{\partial x^2} + \frac{\partial^2 T}{\partial y^2}\right) + \dot{q} \qquad (3.3)$$

The applied boundary condition for the heat transfer problem in Cartesian coordinates is given below; where $\frac{\partial T}{\partial n}$ is the heat flowing normally out of the surface.

$$\left.\frac{\partial T}{\partial n}\right|_{(x=0,y)\ \ t} = 0 \qquad (3.4a)$$

$$\left.\frac{\partial T}{\partial n}\right|_{(x,y\ \ |(x^2+y^2)^{\frac{1}{2}}),\ \ t} = 0 \qquad (3.4b)$$

The initial condition is set at

$$T|_{(x,y),\ \ t=0} = T_{fin} \qquad (3.4c)$$

3.1.2 Cylindrical Formulation

In cylindrical coordinates

$$\nabla^2 T = \frac{1}{r}\frac{\partial}{\partial r}\left(r\frac{\partial T}{\partial r}\right) + \frac{1}{r^2}\frac{\partial^2 T}{\partial \theta^2} + \frac{\partial^2 T}{\partial z^2}$$

The pellet problem can be modeled as an axisymmetric problem therefore $\frac{\partial^2 T}{\partial \theta^2} = \frac{\partial^2 T}{\partial z^2} = 0$ Hence $\nabla^2 T$ reduces to:

$$\nabla^2 T = \frac{1}{r}\frac{\partial}{\partial r}\left(r\frac{\partial T}{\partial r}\right) \qquad (3.5)$$

Therefore the conduction equation for the axisymmetric pellet problem with constant thermal conductivity is given below;

$$\rho c_p \frac{\partial T}{\partial t} = \frac{K}{r}\frac{\partial}{\partial r}\left(r\frac{\partial T}{\partial r}\right) + \dot{q} \qquad (3.6)$$

The boundary condition for the heat transfer problem in cylindrical coordinates is given below

$$\left.\frac{\partial T}{\partial r}\right|_{r=0,\ t} = 0 \qquad (3.7a)$$

$$\left.\frac{\partial T}{\partial r}\right|_{r=R,\ t} = 0 \qquad (3.7b)$$

The initial condition is set at

$$T|_{r,\ t=0} = T_{fin} \qquad (3.7c)$$

3.2 Mass Transfer

Mass transfer in an adsorbent can be modeled by using two approaches, the first being the linear driving force model and the second being the diffusion model. These two mass transfer models are discussed in detail in the following sections.

3.2.1 Linear Driving Force Model

The linear driving force (LDF) model is a model used to predict the loading of an adsorbent, this model is a simplified form of the Fickian diffusion (FD) model. The LDF model assumes a uniform adsorbate concentration (loading) over the entire pellet and then predicts the rate of change of the loading as a function of the difference between the loading and the equilibrium loading at the given adsorption temperature and vapour pressure.

The equation for the LDF is given below:

$$\frac{dX}{dt} = K_{ldf}(X^* - X) \qquad (3.8)$$

Where K_{ldf} is the linear driving force constant and X^* is obtained from an isotherm (eg. Henry's law or Toth's isotherm) the Henry's Law is given by:

$$X = KP \qquad (3.9)$$

Where $K = K_o exp\left(^{Q}/_{R_g T}\right)$

K_o is the pre-exponent factor, $R_g$is the gas constant of the vapour being adsorbed, Q is the heat of adsroption, T is the adsorbent temperature, and P is the partial vapour pressure of the adsorbate (or the evaporator pressure)

The Toth's isotherm is given by equation (3.10)

$$X^* = \frac{K_o exp\left[\frac{Q}{R_g T}\right] P}{\left[1+\left\{\left(\frac{K_o}{W_o}\right) exp\left[\frac{Q}{R_g T}\right] P\right\}^{t'}\right]^{\frac{1}{t'}}} \qquad (3.10)$$

Where W_o is the monolayer capacity and $t'$is the Toth parameter.

At low pressures (and X^*) the Toth isotherm reduces to the Henry's law.

3.2.2 Diffusion Model

Mass transfer during the adsorption model can also be modeled by the Fickian diffusion. For the Fickian diffusion model there is a spatial variation in concentration of the adsorbate over the adsorbent as given by Fick's second law

$$\frac{\partial C}{\partial t} = D_{app}^{pore} \nabla^2 C. \qquad (3.11)$$

Where C is the concentration and D_{app}^{pore} is the apparent diffusivity of pore diffusion

The form of the Fick's second law shown above is normally used for pore diffusion, in which the mass transfer is a bulk diffusion process. Pore diffusion takes place in macroporous adsorbents. The Fick's second law can be expressed in another form which is used for surface diffusion as shown in equation(3.12), this form is expressed in terms of the pellet loading. In surface diffusion the mass transport takes place over the surface of the material, and this form of diffusion takes place in microporous adsorbent of which silica gel is a type. Therefore this form would be employed in the rest of this report.

$$\frac{\partial X}{\partial t} = D_{app}^{surf} \nabla^2 X \qquad (3.12)$$

Where X is the pellet loading and $\mathrm{D_{app}^{surf}}$ is the apparent diffusivity for surface diffusion

The apparent diffusivity is dependent on the pore diffusivity, surface diffusivity and the constant $K = \frac{\partial X}{\partial p}$ which is the slope of the isotherm, as stated by [10], the apparent diffusivity is given as;

$$D_{app}^{surf} = \frac{\varepsilon D_P + (1-\varepsilon) K D_s}{\varepsilon + (1-\varepsilon) K} \qquad (3.13)$$

According to Raymond and Garimella [20] when surface diffusion dominates the apparent diffusivity can be approximated as

$$D_{app}^{surf} = \frac{(1-\varepsilon) K D_s}{\varepsilon + (1-\varepsilon) K} \qquad (3.14)$$

And for high values of K, which is usually of the order of 10 to 1000; Raymond and Garimella[20] reporting Do[10], the apparent diffusivity can be approximated as the surface diffusivity.

$$D_{app}^{surf} \approx D_s \tag{3.15}$$

The diffusion equation expressed in Cartesian coordinates is given below

$$\frac{\partial X}{\partial t} = D_{app}^{surf}\left(\frac{\partial^2 X}{\partial x^2} + \frac{\partial^2 X}{\partial y^2}\right) \tag{3.16}$$

with the following boundary and initial conditions

$$\left.\frac{\partial X}{\partial n}\right|_{(x=0,y)\ \ t} = 0 \tag{3.17a}$$

$$X|_{\substack{(x,y\ \ |(x^2+y^2)^{\frac{1}{2}}),\ \ t}} = X^*|_{T_{ads},\ P_{evap}} \tag{3.17b}$$

The initial condition is set at

$$X|_{(x,y),\ \ t=0} = 0 \tag{3.17c}$$

The diffusion equation expressed in cylindrical coordinates is given below

$$\frac{\partial X}{\partial t} = \frac{D_{app}^{surf}}{r}\frac{\partial}{\partial r}\left(r\frac{\partial X}{\partial r}\right) \tag{3.18}$$

The boundary conditions of the pellet as shown by Raymond and Garimella[20] can be set as shown below:

$$\left.\frac{\partial X}{\partial r}\right|_{r=0,\ \ t} = 0 \tag{3.19a}$$

$$X|_{r=R,\ \ t} = X^*|_{T_{ads},\ P_{evap}} \tag{3.19b}$$

The initial condition is set at

$$X|_{r,\ \ t=0} = 0 \tag{3.19c}$$

3.3 Coupled Heat and Mass Transfer Equations

3.3.1 LDF Model

The heat and mass transfer processes can then be coupled as shown below:

The volumetric heat generation in the pellet is a function of the rate of loading obtained from the LDF, and is given by the equation (3.8) below.

$$\dot{q} = Q\rho\frac{dX}{dt} = Q\rho K_{ldf}(X^* - X) \tag{3.20}$$

when the volumetric heat generation equation is coupled with the heat conduction equation given in equation(3.4) the resulting coupled equation is given below:

$$\rho c_p\frac{\partial T}{\partial t} = k\nabla^2 T + Q\rho K_{ldf}(X^* - X) \tag{3.21}$$

where Q is the heat of adsorption and ρ is the pellet density.

This equation can be expressed in Cartesian coordinates as:

$$\rho c_p \frac{\partial T}{\partial t} = k\left(\frac{\partial^2 T}{\partial x^2} + \frac{\partial^2 T}{\partial y^2}\right) + Q\rho K_{ldf}(X^* - X) \quad (2.22)$$

or in cylindrical coordinates as:

$$\rho c_p \frac{\partial T}{\partial t} = \frac{k}{r}\frac{\partial}{\partial r}\left(r\frac{\partial T}{\partial r}\right) + Q\rho K_{ldf}(X^* - X) \quad (3.23)$$

3.3.2 Diffusion Model

The mass and heat transfer models can then be coupled in a similar way for the Diffusion model as was done for the LDF model.

The volumetric heat generation is given as

$$\dot{q} = Q\rho\frac{\partial X}{\partial t} = Q\rho D_{app}^{surf}\nabla^2 X \quad (3.24)$$

This can be expressed in Cartesian coordinates as

$$\dot{q} = Q\rho\frac{\partial X}{\partial t} = Q\rho D_{app}^{surf}\left(\frac{\partial^2 X}{\partial x^2} + \frac{\partial^2 X}{\partial y^2}\right) \quad (3.25)$$

or in cylindrical coordinates as

$$\dot{q} = Q\rho\frac{\partial X}{\partial t} = Q\rho\frac{D_{app}^{surf}}{r}\frac{\partial}{\partial r}\left(r\frac{\partial X}{\partial r}\right) \quad (3.26)$$

When the mass transfer is coupled with the heat transfer by including the volumetric heat generation term given in equation(3.24) in the conduction equation, the coupled heat and mass PDE is given in equation(3.27).

$$\rho c_p \frac{\partial T}{\partial t} = k\nabla^2 T + Q\rho D_{app}^{surf}\nabla^2 X \quad (3.27)$$

The coupled PDE for the is expressed below for the Cartesian case

$$\rho c_p \frac{\partial T}{\partial t} = k\left(\frac{\partial^2 T}{\partial x^2} + \frac{\partial^2 T}{\partial y^2}\right) + Q\rho D_{app}^{surf}\left(\frac{\partial^2 X}{\partial x^2} + \frac{\partial^2 X}{\partial y^2}\right) \quad (3.28)$$

The coupled PDE equation can also be expressed in cylindrical coordinates for the axisymmetric case as shown below:

$$\rho c_p \frac{\partial T}{\partial t} = \frac{K}{r}\frac{\partial}{\partial r}\left(r\frac{\partial T}{\partial r}\right) + Q\rho\frac{D_{app}}{r}\frac{\partial}{\partial r}\left(r\frac{\partial X}{\partial r}\right) \quad (3.29)$$

These coupled heat and mass transfers would then be solved using the solvers in PDE Toobox of Matlab or those developed by Tierney, M.J[31].

CHAPTER 4 FINITE ELEMENT MODELS

In order to simulate the problem, models were created using the finite element method, three models were created. The first two models use the liner driving force method to model the adsorption process, while the last model uses Fickian diffusion to model the adsorption process. Both models are coupled heat and mass transfer problems, with the mass transfer causing a volumetric heat generation and the temperature gradients having an effect on the rate of adsorption.

The models created is described in detail in the following sections.

4.1 Model Geometry and Mesh

4.1.1 Geometry

The three dimensional model of the pellet and the bond attached to a fin was reduced to a two dimensional model for the following reasons.

- The heat transfer and adsorption process can be accurately represented as an axisymmetric problem [32].
- 2 dimensional model are cheaper in terms of computational costs.
- It would also be easier to view the results of the simulation in 2 dimensions than it would be in 3 dimensions, and because of the geometry of the model, the two dimensional plots of the section would give a complete representation.
- The solvers to be used (Matlab PDE Toolbox and Java Routines developed by Dr M. J. Tierney [31]) only solves the 2 dimensional problem. More elaborate finite element applications would have been employed, but they do not provide the type of flexibility and control which these two solvers provide.

The geometry was represented by a half pellet in two dimensions as shown in the Figure 4.1 below:

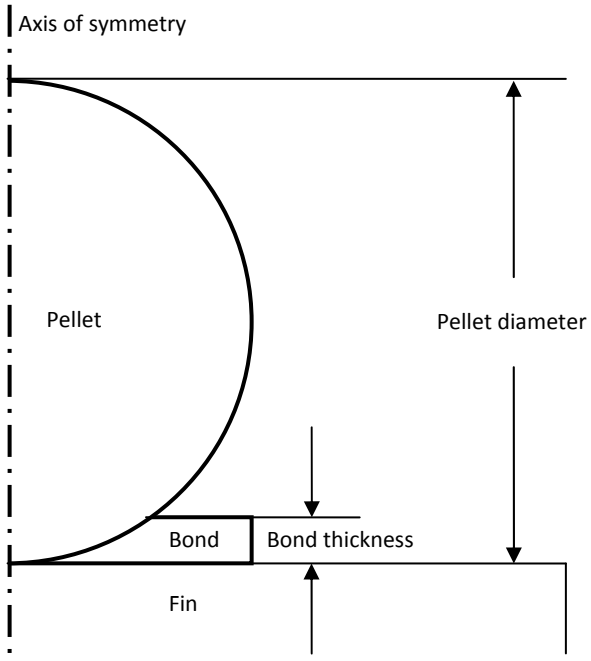

Figure 4.1 Model geometry

4.1.2 Mesh

The model is meshed using a Delaunay triangulation algorithm in Matlab'S PDE toolbox[33]. The meshing algorithm creates an unstructured mesh over the entire domain. This algorithm also possesses some form of automatic mesh refinement, as it creates elements of variable sizes depending on the geometry being meshed. Two meshes are shown in Figure 4.2 the mesh near the bond on the right was automatically refined to cater for the small bond thickness.

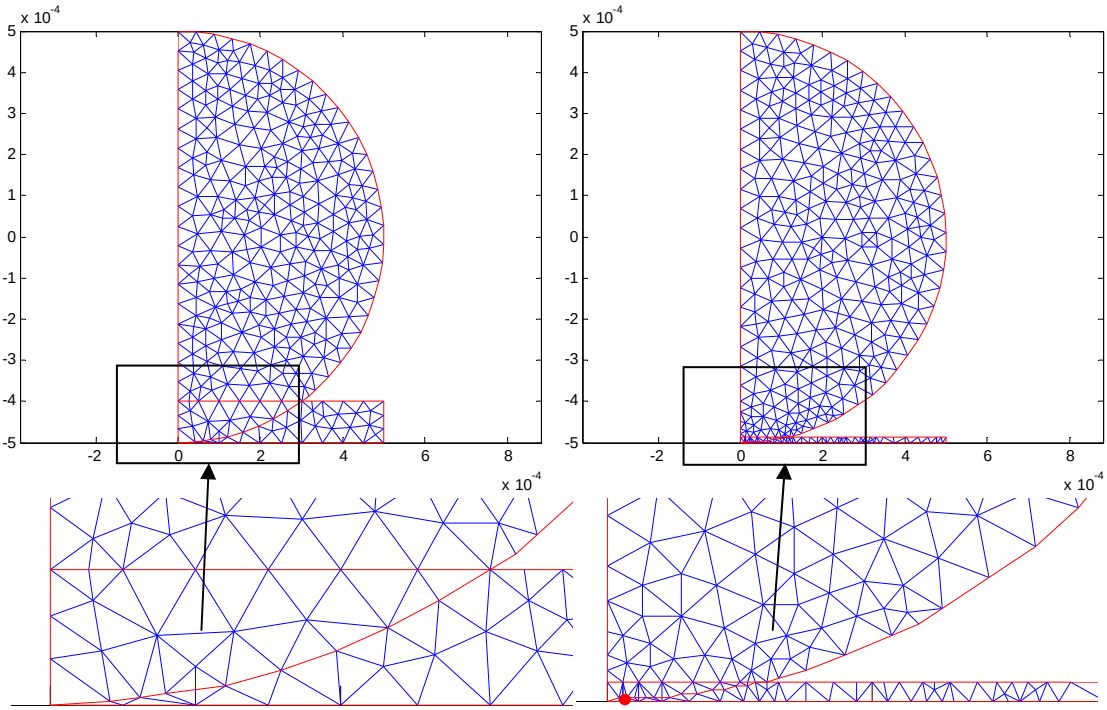

(a) (b)

Figure 4.2 Mesh of model showing automatic mesh refinement by Delaunay meshing algorithm (a) Model with basic mesh (b) Model with automatically refined mesh due to presence of small feature

4.2 Model Boundary Conditions

Surf. No	Surface	Heat Transfer B/C	Mass Transfer B/C	Notes
(1)	Axis of symmetry	Adiabatic Eqn. 3.4a	Zero flux 3.17a	Due to the symmetry of the system the net heat or mass flux across the central axis is zero
(2)	Pellet surface	Adiabatic Eqn. 3.4b	Constant concentration (or loading) Eqn. 3.17b	The loading on the pellet surface is assumed constant according to work carried out by Raymond and Garimella[20]
(3)	Bond surface	Adiabatic	Zero flux	The bond is assumed to be impermeable to the adsorbate
(4)	Contact surface between bond and fin	Isothermal	Zero flux	In terms of heat transfer, the thermal conductivity of aluminium is much greater than that of the pellet, therefore the temperature gradient at the contact can be assumed to be zero. In terms of mass transfer; the contact surface is assumed to have no contact with the adsorbate, and on the other hand; the bond is impermeable to the adosrbate.

Table 4.1 Description of applied boundary conditions

The applied boundary conditions for the model shown in Figure 4.3 and is described in detail in Table 4.1

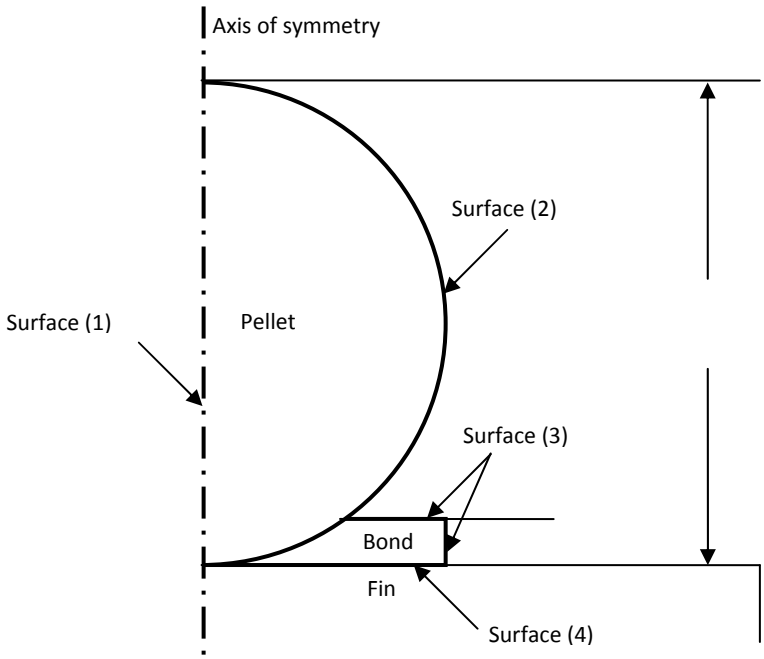

Figure 4.3 Model geometry showing different surfaces (Refer to Table 4.1 for applied thermal and mass transfer boundary)

4.3 Finite Element Formulation

Two methods were used to create the finite element models, the first of these was done by creating Cartesian finite elements, while the other used axisymmetric finite elements. The Cartesian method used Matlab's PDE Toolbox facilities, while the axisymmetric uses own code (developed by Tierney, M.J)

	LDF mass transfer model	Diffusion mass transfer model
Cartesian finite element (Matlab)	CART LDF	CART Diffusion
Axisymmetric finite element (Tierney, M.J [31])	AXI LDF	

Table 4.2 Classification of finite element formulations used

CART LDF, means the linear driving force model formulated using Matlab's PDE Toolbox Cartesian element, the same goes for diffusion; the diffusion model formulated using Matlab's PDE Toolbox Cartesian element formulation. AXI LDF; means the LDF model formulated using the axisymmetric element developed by Tierney, M.J [31].

The axisymmetric finite element formulation was carried out by using triangular 3-noded elements with C^o continuity.(according to Lewis et.al [34] for details) The finite element formulation was then solved using the Galerkin method.

The Cartesian formulation uses Matlab's PDE Toolbox functionality.

4.4 Description of Finite Element Simulation

A brief description of the simulation is given in this section, two models were produced, the LDF and the Diffusion models. The main difference between these two models is how the volumetric heat generation is determined, as this depends on the mass transfer model used.

4.4.1 The Linear Driving Force Simulation

The linear driving force model was created by coupling the LDF model which is used to determine the loading of the pellet with a heat transfer model for the pellet as shown in section 3.2.1.

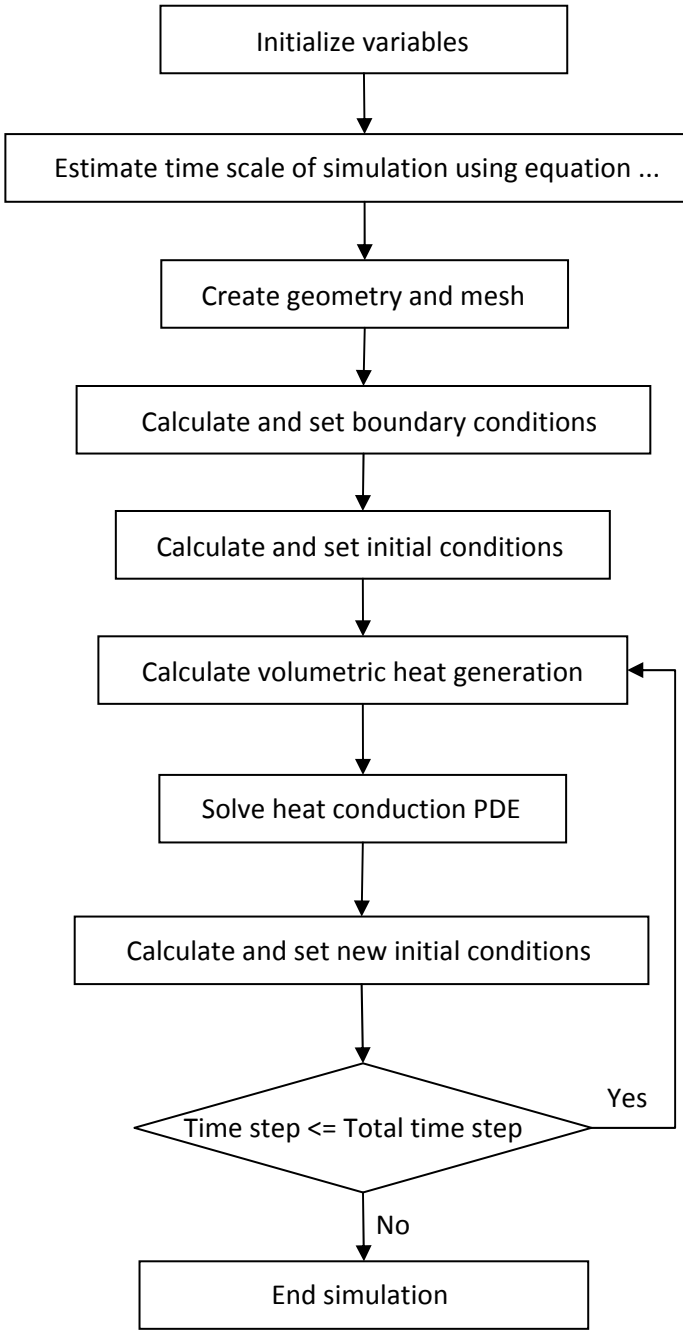

Figure 4.4 Simulation flow for LDF model

4.4.2 The Diffusion Simulation

In a similar way the Diffusion model was created by coupling the Diffusion model with the heat transfer model as shown below.

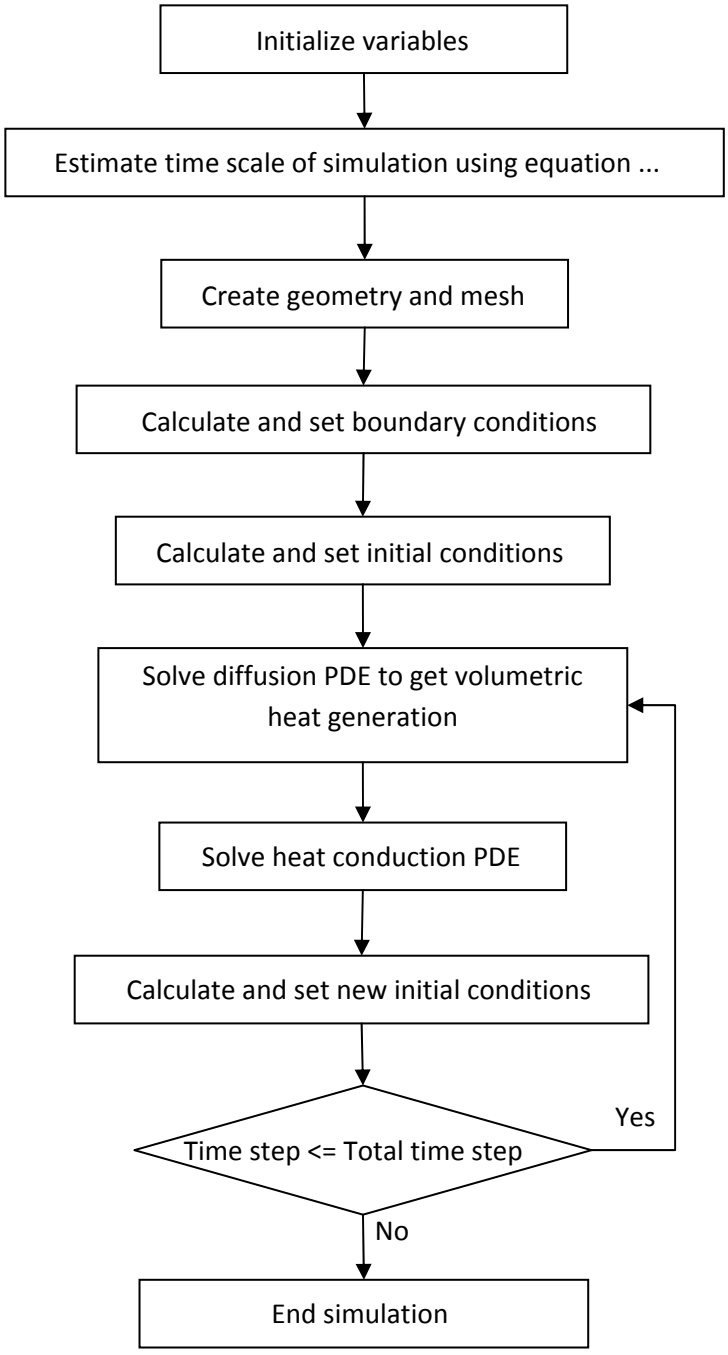

Figure 4.5 Simulation flow for diffusion model

4.5 Effect of Simulation Parameters on Simulation Result

This section tests the effect of some simulation parameters on the result of the simulation, the two parameters tested are the mesh size and the time step.

4.5.1 Effect of Mesh Size

In order to check the effect of mesh refinement on solution accuracy, the simulation was carried out with increasingly fine meshes. The mesh was refined by setting the maximum edge length to a value "Edge ratio for mesh" which is a fraction of the radius of the pellet.

$$maximum\ edge\ length\ for\ mesh\ element = \frac{radius\ of\ pellet}{edge\ ratio\ for\ mesh} \qquad (4.1)$$

The value of edge ratio for mesh was varied between the value of 4 and 20, in steps of 2.

The residual values for the mean pellet loading and temperature was then calculated over the entire time period, and the average obtained, based on equation (4.2) below.

$$Residual(i) = \frac{\sum_j^n \left[X_j^{(i+1)} - X_j^{(i)}\right]}{n} \qquad (4.2)$$

where i: represnets the ith simulation with the ith value of edge ratio, j: is the data point, and n: is the total number of data points, X: is the measurement e.g. temperature or loading

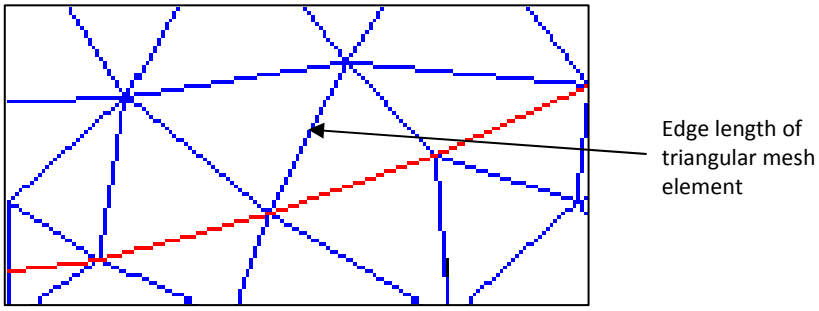

Figure 4.6 Portion of mesh showing triangular element and edge length

Edge ratio	4-6	6-8	8-10	10-12	12-14	14-16	16-18	18-20
AXI LDF	-1.49E-05	-9.94E-06	-3.12E-05	-1.69E-05	-2.21E-05	-2.22E-05	-2.62E-05	-2.71E-05
CART LDF	-1.65E-05	-5.57E-06	-1.64E-05	-1.38E-06	-3.27E-06	-2.52E-06	-2.01E-06	-1.56E-06
CART Diffusion	-0.00017	-0.0001	-8.83E-05	2.50E-06	-1.45E-05	-6.78E-06	-9.27E-06	-1.77E-06

Table 4.3 Mean loading residuals as edge ratio was increased

Edge ratio	4-6	6-8	8-10	10-12	12-14	14-16	16-18	18-20
AXI LDF	0.001218	-0.00035	0.001601	-0.0003	0.000195	0.000193	0.000141	0.000112
CART LDF	0.002733	0.000928	0.002724	0.000229	0.000543	0.000418	0.000335	0.00026
CART Diffusion	0.0027	0.000928	0.00268	0.000225	0.000523	0.000405	0.000338	0.000239

Table 4.4 Mean temperature residuals as edge ratio was increased

From the plots of loading and temperature against time (Figure 4.7) it can be observed that the mesh size does not have a significant effect on the solution results. The plots of residuals against edge ratio

for the mesh also suggests this. For the loading residuals, the residual values were of the order of 10^{-5} kg/kg, for edge ratios greater than 10, and the temperature residuals gave values of the order of 10^{-3} K. The temperature residuals is roughly of the same order as that of the loading, if we consider the ratio of the temperature residual to the actual temperature; as the temperature is of the order of 10^{2}, giving a temperature residual ratio of the order of 10^{-5}, and a loading residual ratio of the order 10^{-5} also, as the actual loading is of the order of 10^{0}.

From the results above we observed that mesh edge ratios of about 10 and above gave results of reasonable accuracy, and increased edge ratios resulted in better convergence of the solution. A value of 10 was chosen for the edge ratio in the simulation in order to provide a good balance between solution accuracy and computational cost.

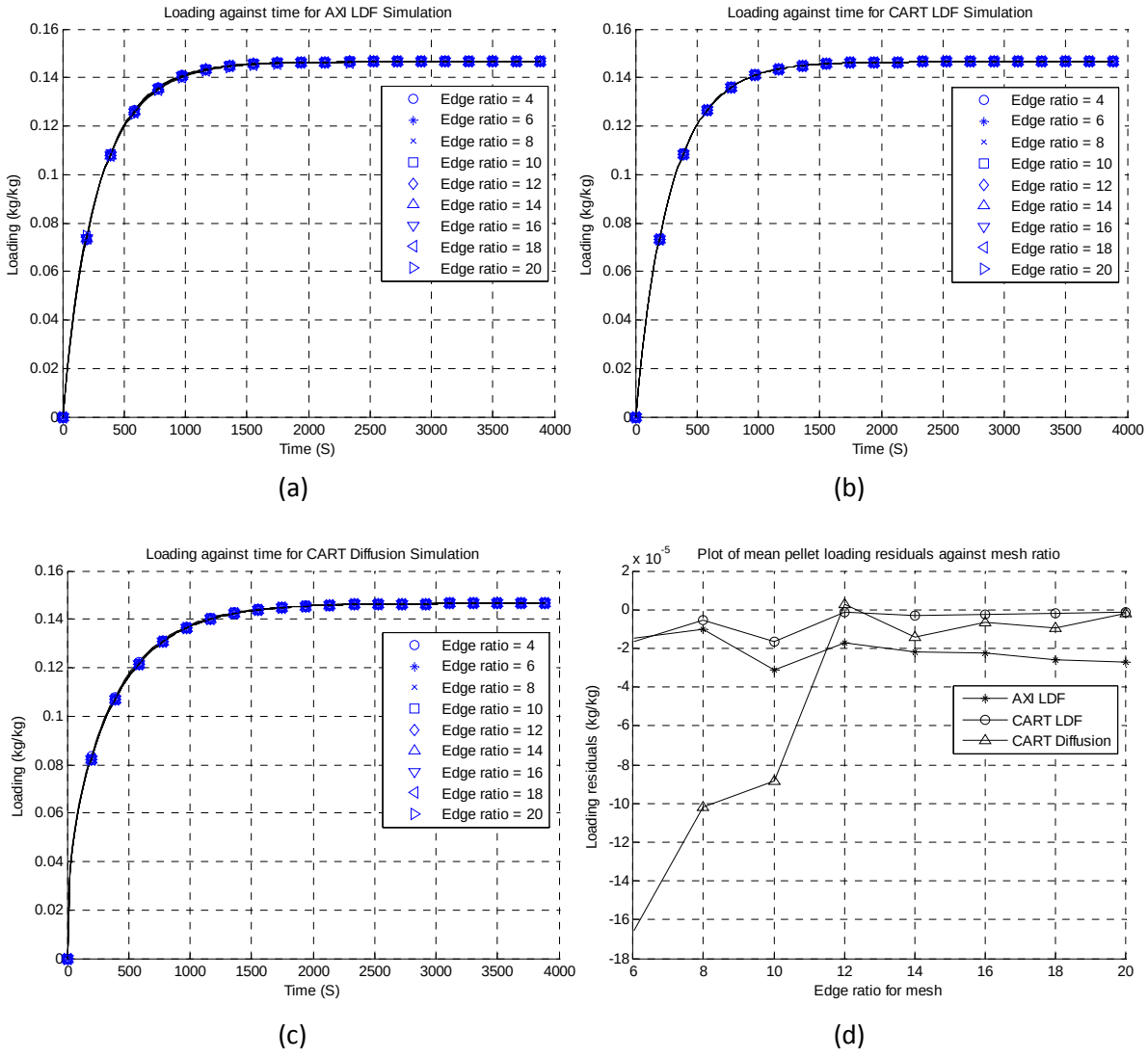

Figure 4.7 Plot of loading against time and residual for different mesh edge ratios (a)For AXI LDF simulation (b) For CART LDF simulation (c) For CART Diffusion simulation (d) Plot of loading residuals for the 3 models.

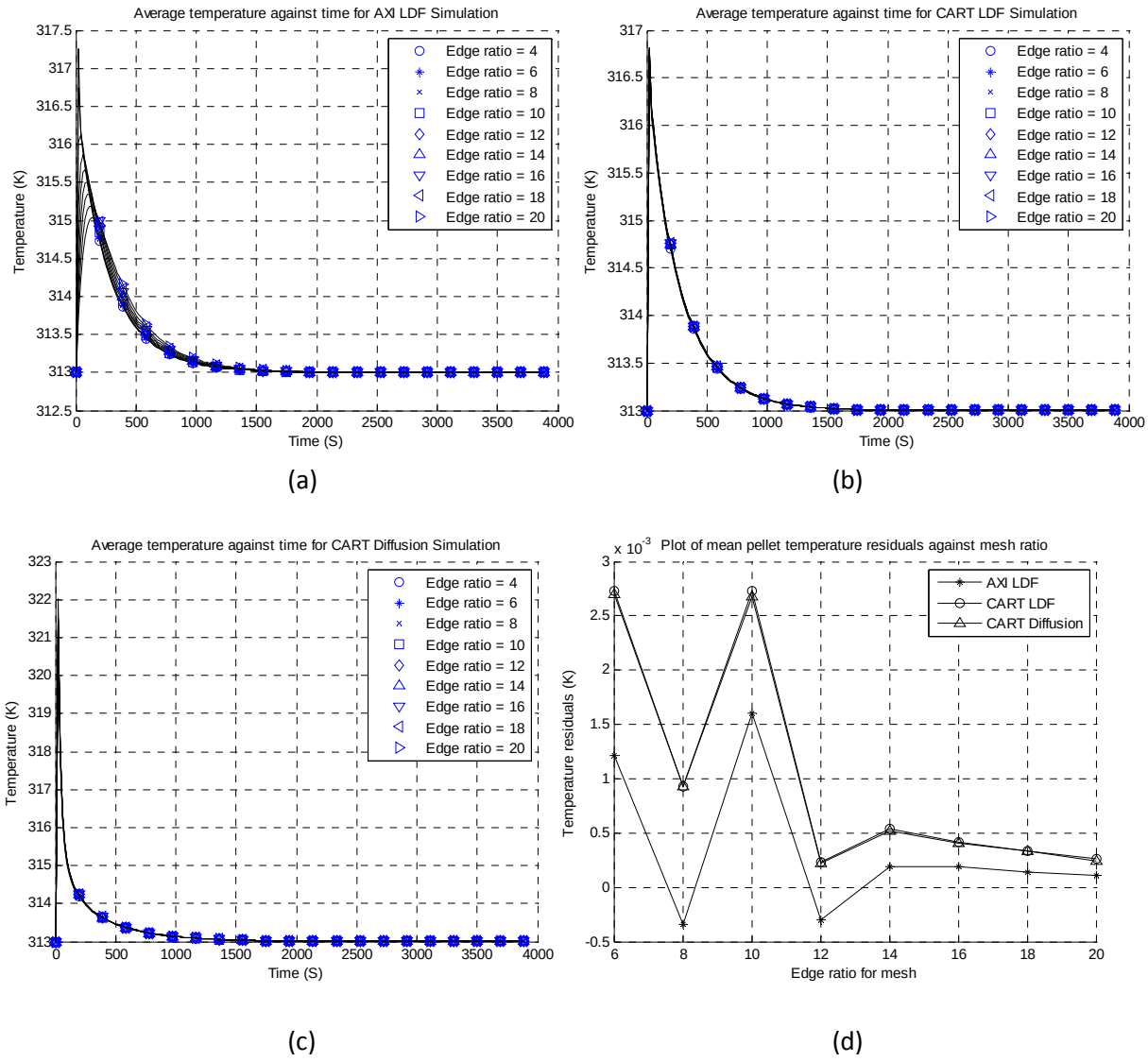

Figure 4.8 Plot of temperature against time and residual for different mesh edge ratios (a)For AXI LDF simulation (b) For CART LDF simulation (c) For CART Diffusion simulation (d) Plot of temperature residual for the 3 models

4.5.2 Effect of Time Step

Using a similar approach to that used for the mesh refinement check, the effect of time steps was also investigated. The simulation was carried out repeatedly with the same parameters and the time step was varied between 50 and 4000. The effect of varying time steps on the solution accuracy was then investigated. The results (as shown in Figures 4.9 and 4.10) indicate that the solution converges as the number of time steps was increased.

The time step is the number of interval into which the total simulation time is divided.

The residuals for these simulations was calculated using equation 4.2, and plotted in Figures 4.9(d) and 4.10(d), The obtained values for the residual is shown in the Tables 4.5 and 4.6.

Time step	50-100	100-150	150-200	200-400	400-600	600-800	800-1000	1000-2000	2000-4000
AXI LDF	-0.00106	-0.00038	-0.00017	-0.00026	-8.63E-05	-4.28E-05	-2.56E-05	-5.17E-05	-2.76E-05
CART LDF	-0.00119	-0.00043	-0.0002	-0.00031	-0.0001	-5.17E-05	-3.12E-05	-6.32E-05	-3.20E-05
CART Diffusion	-0.00104	-0.00057	-0.00027	-0.00044	-0.00015	-7.62E-05	-4.65E-05	-9.78E-05	-3.74E-05

Table 4.5 Mean loading residuals as time step was increased

Time step	50-100	100-150	150-200	200-400	400-600	600-800	800-1000	1000-2000	2000-4000
AXI LDF	-0.00306	-0.00546	-0.00174	-0.00578	-0.00297	-0.00173	-0.00109	-0.00217	-0.00089
CART LDF	-5.11E-07	-0.00807	-0.00631	-0.00285	-0.00103	-0.00042	-0.0002	-0.00027	-4.73E-05
CART Diffusion	7.17E-07	-0.0193	-0.01539	-0.02684	-0.0076	-0.00279	-0.00127	-0.00178	-0.00092

Table 4.6 Mean temperature residuals as time step was increased

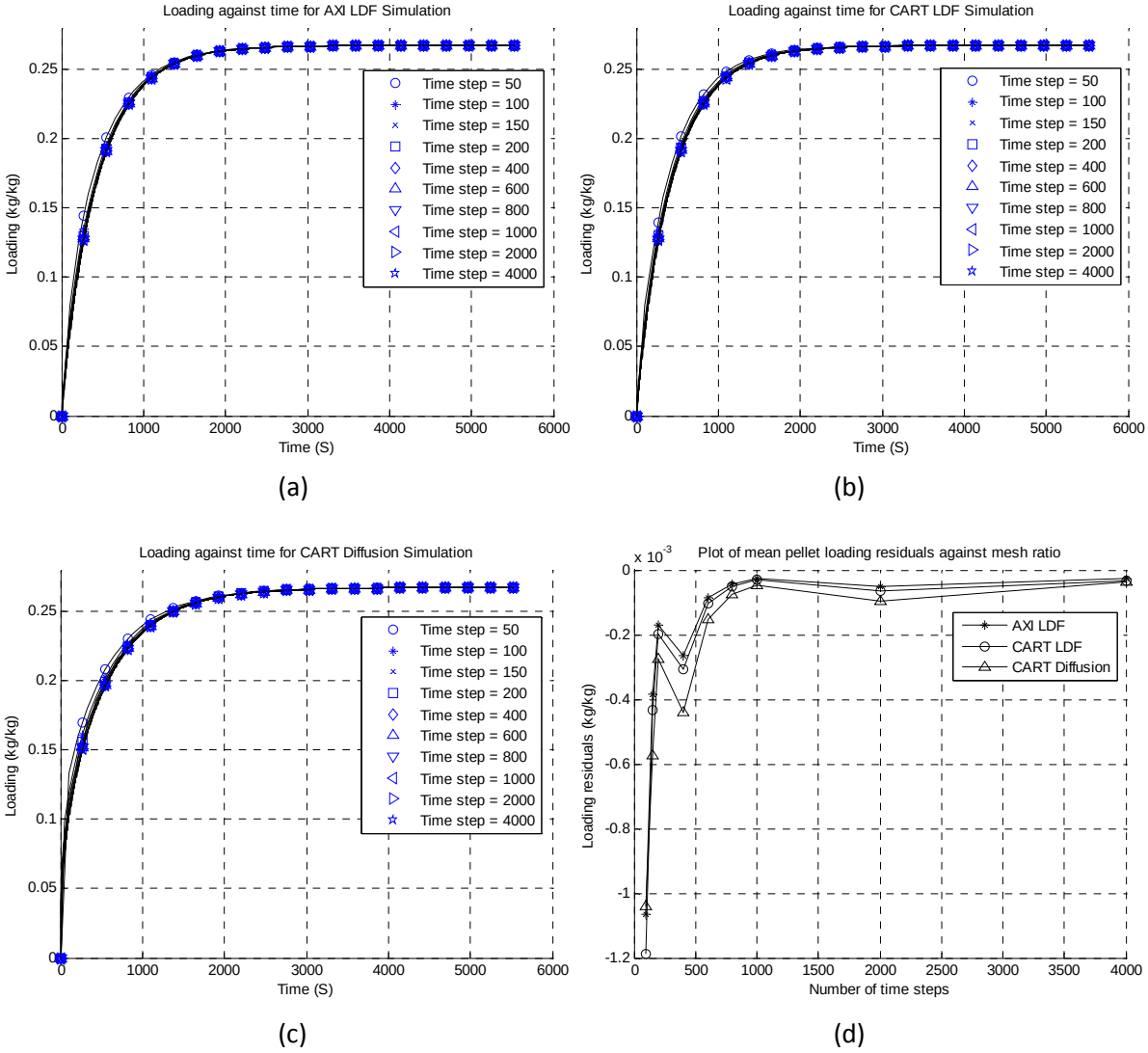

Figure 4.9 Plot of loading against time and residual for different time steps (a)For AXI LDF simulation (b) For CART LDF simulation (c) For CART Diffusion simulation (d) Plot of loading residuals for the 3 models

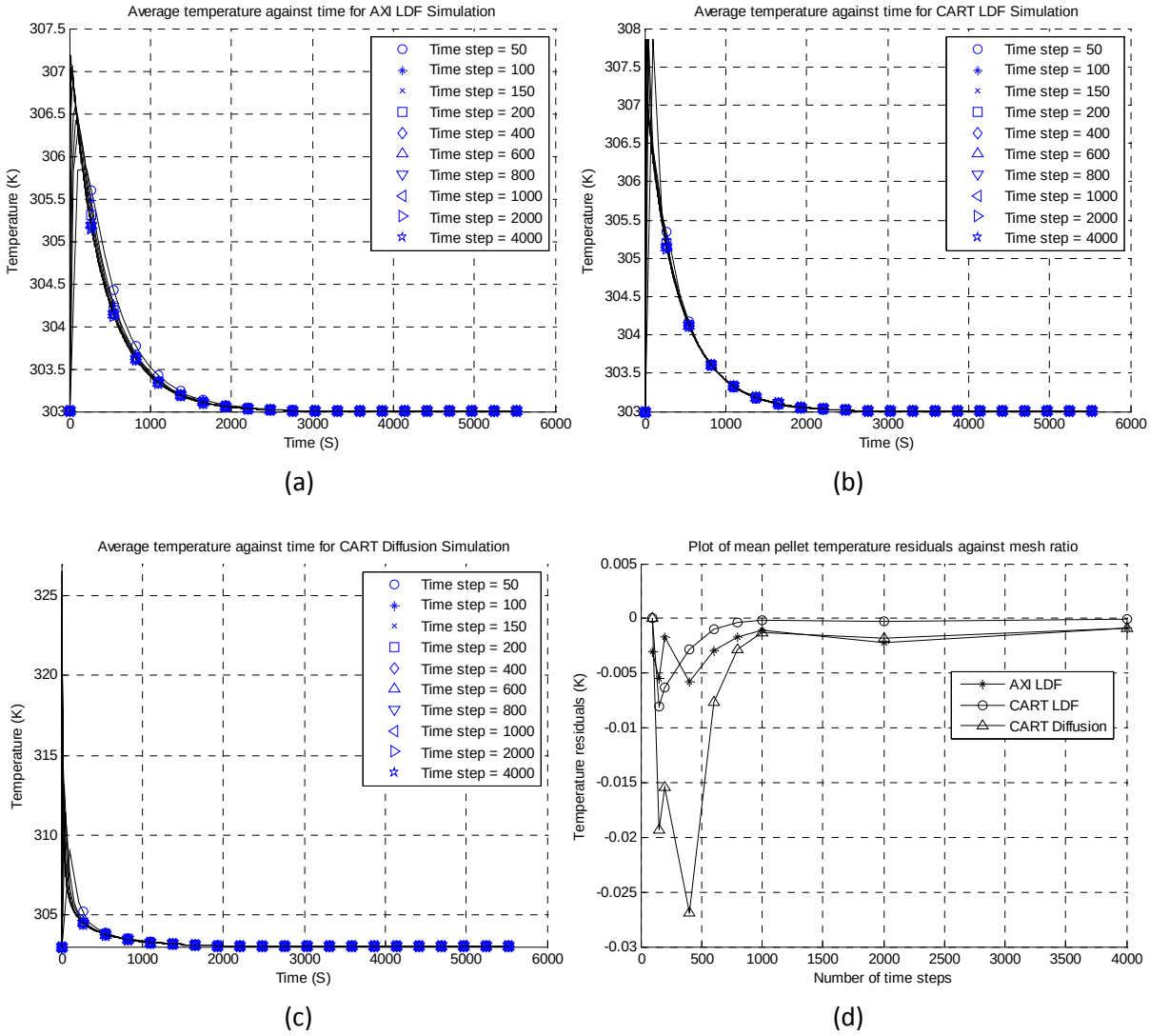

Figure 4.10 Plot of temperature against time and residual for different time steps (a)For AXI LDF simulation (b) For CART LDF simulation (c) For CART Diffusion simulation (d)Plot of temperature residuals for the 3 models

From the plots shown above (Figure 4.9 and 4.10), it was observed that the time step had a greater effect on the solution than the mesh size

The results in Figures 4.9 and 4.10 & Tables 4.5 & 4.6 above show that the solution converges as the time step is increased. When the time step was increased above 100, very little changes was noticed in the solution result, this suggests that at time steps of 1000 and above, the solution is reasonably converged. Therefore a time step of near this value would be chosen to give a good balance between solution accuracy and computational cost.

4.6 Consistency Checks

The created finite element model was checked for computational accuracy by comparing against other models and against experimental result. The performance of the model was also checked under varying conditions for example the effect of varying mesh size and varying time steps was also checked. The result of the verification phase is discussed in detail in the following sections.

Property (Unit)	Value[1]
Silica gel type	Type A
Thermal conductivity of pellet (W/mK)	0.174
Thermal conductivity of bond (W/mK)	0.2
Density of pellet (kg/m^3)	1306
Density of bond (kg/m^3)	1200
Heat capacity of pellet (J/kgK)	921
Heat capacity of bond (J/kgK)	1000
Heat transfer coefficient of pellet (W/m^{2}K)	0
Heat transfer coefficient of bond (W/m^{2}K)	0
Radius of pellet (m)	5.00E-04
Thickness of bond (m)	0.0001
Heat of adsorption (J/kg)	2.69E+06
Activation energy (J/mol)	4.20E+04
Fin temperature (K)	303
Ambient temperature (K)	297.0978
Initial temperature (K)	303
Geometric factor	15
Surface diffusivity at zero loading	2.54E-04
Molar gas constant (J/mol)	8.3145
Molar mass of adsorbate (kg/kmol)	18
Henry's constant at zero loading(Pa^{-1})	5.9E-13
Monolayer adsorption capacity (kg/kg)	0.4
Toth parameter	12

Table 4.7 Base parameters for simulation

4.6.1 Verification of Equilibrium Loading Values Attained by Model

The created model would be compared with experimental results obtained by Ahamat and Tierney[1]

The steps carried out to verify the model are listed below:

- The model was set up using the parameters in Table 4.7.
- The time scale required for the model to attain equilibrium was then estimated from the value of the surface diffusivity .
- The model was then run through the entire time, over a range of temperatures and pressures (for which the results are plotted in Figures 4.12 to 4.14).
- The final value of the loading for each temperature and pressure was extracted, this being the equilibrium loading of the pellet at the given adsorbent temperature and evaporator pressure.
- The results were then plotted as shown in Figures 4.12 to 4.14.

Figure 4.11 shows the result obtained by Ahamat and Tierney[1], while Figures 4.12 to 4.14 shows the results obtained from the simulation. The ratio of the simulation result to the experimental result obtained by Ahamat and Tierney[1] is shown in Figure 4.15.

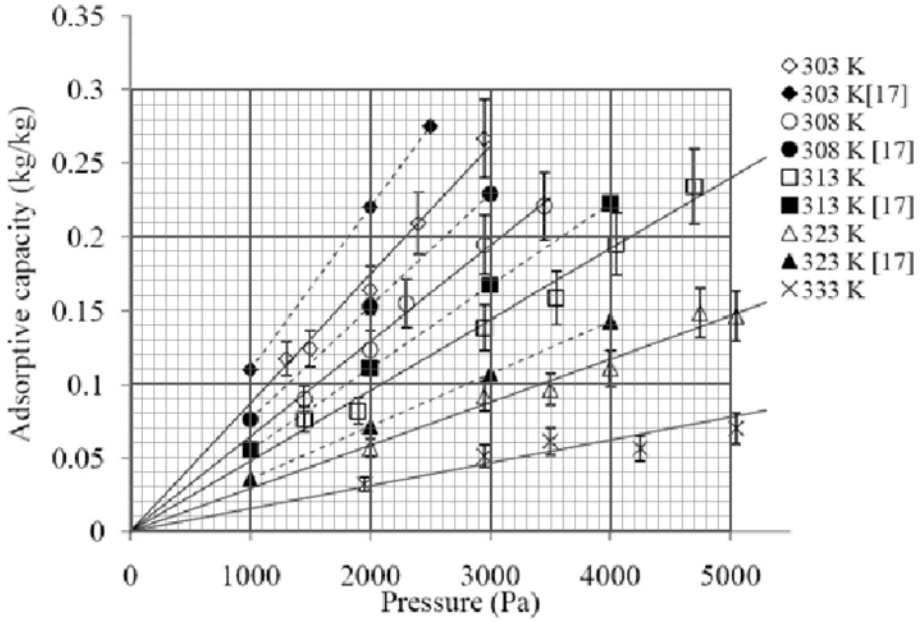

Figure 4.11 Graph of equilibrium uptake for water and Type A silica gel (with overlaid grid for easy data extraction); Ahamat and Tierney [1]

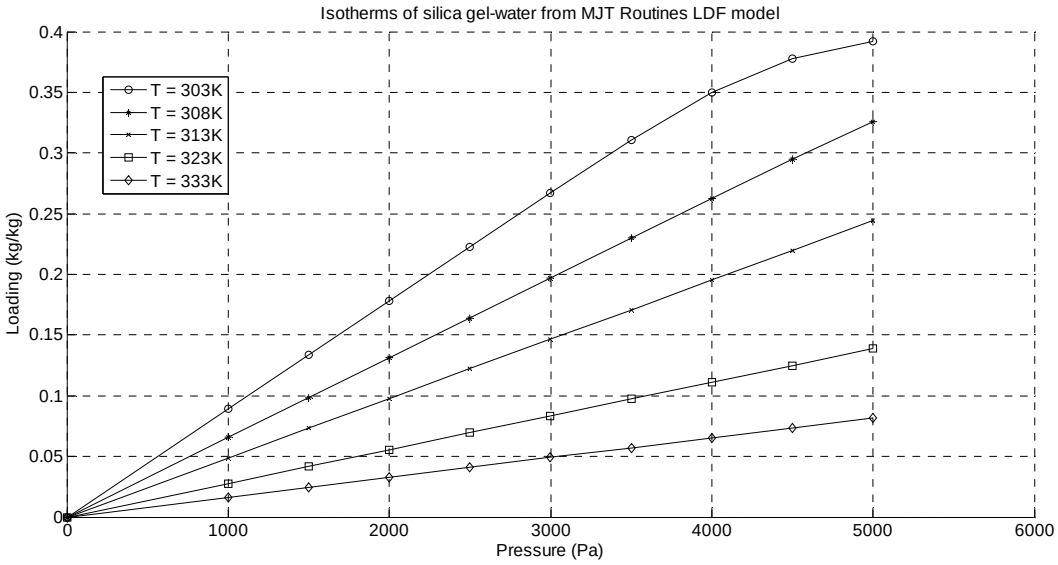

Figure 4.12 Equilibrium uptake for water and Type A silica gel using AXI LDF model

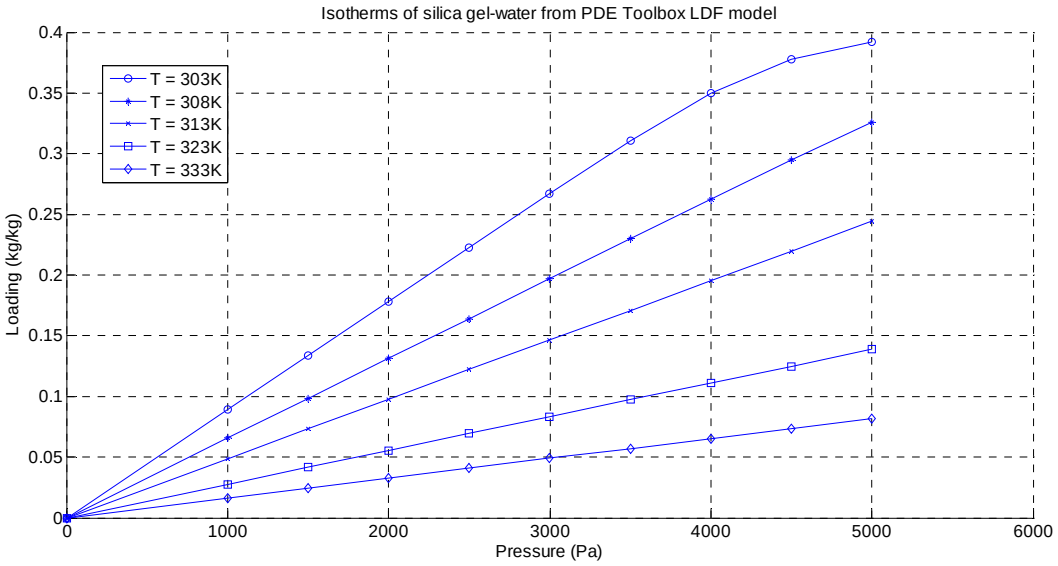

Figure 4.13 Equilibrium uptake for water and Type A silica gel using CART LDF model

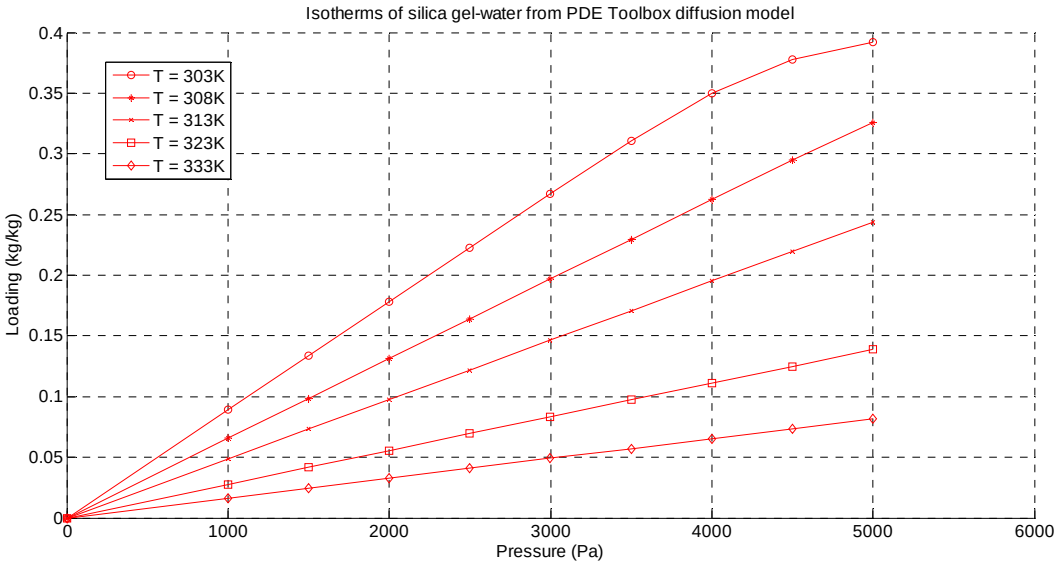

Figure 4.14 Equilibrium uptake for water and Type A silica gel using CART Diffusion model

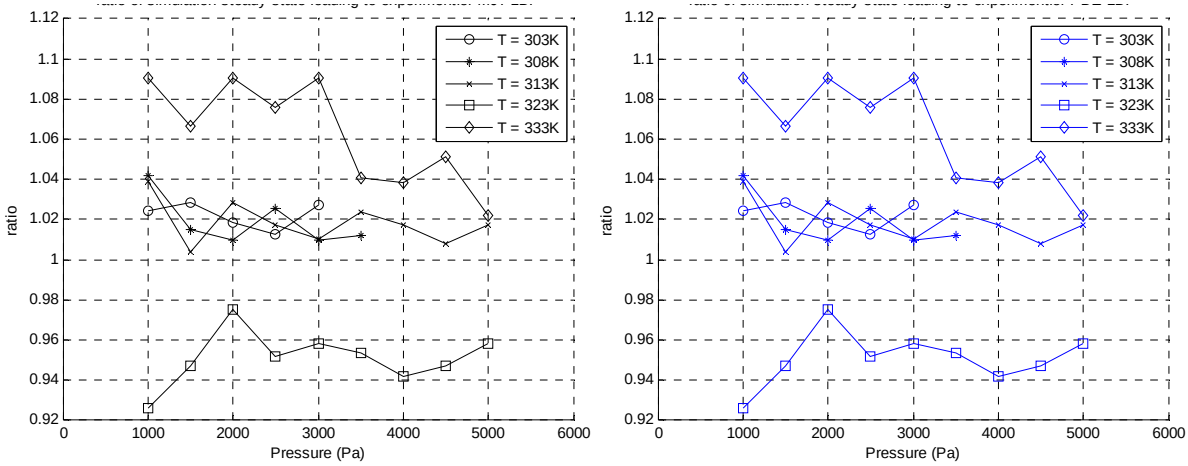

(a) (b)

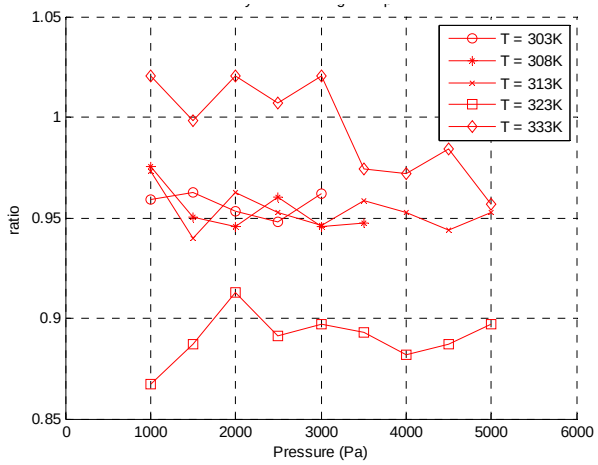

(c)

Figure 4.15 Ratio of simulation results to experimental result
(a)For AXI LDF simulation (b) For CART LDF simulation (c) For CART Diffusion simulation

From the results the model attained approximately the same equilibrium loading as that obtained in the experiment carried out by Ahamat and Tierney [1], with a variation of about ±10% for the LDF and about ±13% for the diffusion model. Hence it can be inferred that the model attains the proper equilibrium loading after the appropriate time scale has been reached.

4.6.2 Verification of Time Taken to Attain a Percentage of Equilibrium Loading

In order to check the transient condition of the model, and ensure it attains the equilibrium loading at the right time, the model would be compared with available experimental data.

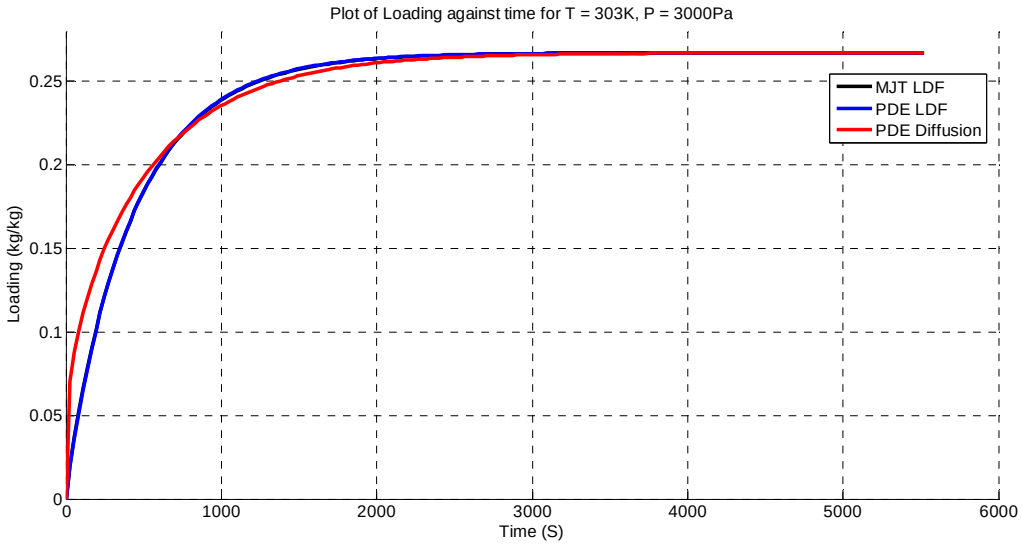

Figure 4.16 Average pellet loading against time for 303K and 3000Pa

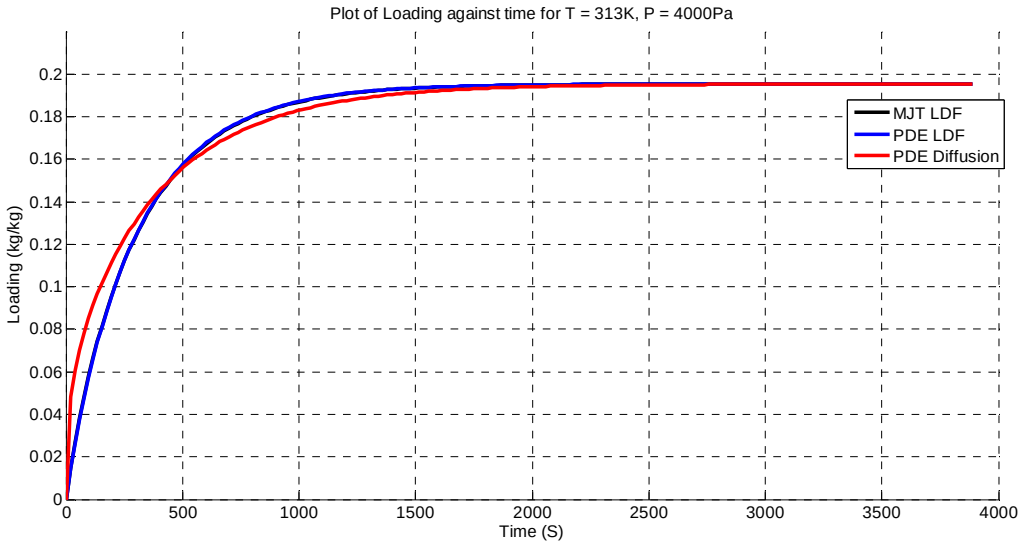

Figure 4.17 Average pellet loading against time for 313K and 4000Pa

The time taken to reach 63.2% of the equilibrium loading capacity is given in Tables 4.8 to 4.10, the values obtained from experiments carried out by Ahamat and Tierney[1] is given in the second column of the tables. As access to the detailed experimental result is unavailable, an approximate value of the time taken to attain 63.2% of the equilibrium loading has been calculated from the Arrhenius plot (Figure 4.18) as given in the paper by Ahamat and Tierney [1], the result of this is shown in Tables 4.8 to 4.10. The result was observed to be in close approximation with the that from the simulation.

The Arrhenius plot by [1] contained values for different pressures, but no indication was given of any relationship between the measured time and the pressure. Therefore the experimental values shown in column 2 of Tables 4.8 to 4.10 is a rough estimate of the time obtained over all pressures.

Further discussion on the possible dependence of adsorption kinetics on pressure is contained in the chapter on tests and results.

	Exp.	1000Pa	1500Pa	2000Pa	2500Pa	3000Pa	3500Pa	4000Pa	4500Pa	5000Pa
303K	383.7	377.9785	389.6666	401.6035	413.142	424.6989	434.0551	435.4879	419.3637	388.0427
308K	314.0	313.281	321.5619	330.0848	338.5094	346.728	355.2312	363.3304	370.5889	375.761
313K	270.0	261.5169	267.5418	273.5335	279.7125	285.7504	291.6679	297.8374	303.8553	309.6931
323K	190.6	185.8105	189.081	192.2952	195.4562	198.7783	202.057	205.2806	208.4521	211.7061
333K	134.3	135.1119	136.9448	138.7533	140.5383	142.3009	144.08	145.9248	147.7453	149.5424

Table 4.8 Time to reach 63.2% of the equilibrium loading for AXI LDF Simulation

	Exp.	1000Pa	1500Pa	2000Pa	2500Pa	3000Pa	3500Pa	4000Pa	4500Pa	5000Pa
303K	383.7	377.6511	389.0911	400.7922	412.0848	423.315	432.4533	433.8149	417.97	387.3746
308K	314.0	313.0494	321.1834	329.5115	337.7613	345.7848	354.0505	361.965	368.9923	373.9936
313K	270.0	261.3505	267.2713	273.1216	279.177	285.0853	290.8586	296.8454	302.724	308.425
323K	190.6	185.721	188.9372	192.0921	195.1899	198.4268	201.6345	204.7858	207.8835	211.0201
333K	134.3	135.0615	136.8649	138.6412	140.3919	142.1221	143.8485	145.6533	147.4328	149.1882

Table 4.9 Time to reach 63.2% of the equilibrium loading for CART LDF Simulation

	Exp.	1000Pa	1500Pa	2000Pa	2500Pa	3000Pa	3500Pa	4000Pa	4500Pa	5000Pa
303K	383.7	375.9214	368.3021	360.2964	352.2131	343.8904	335.3012	327.3685	321.5794	318.616
308K	314.0	322.6304	317.4731	312.106	306.5418	300.7406	294.9745	289.0285	282.8913	276.7641
313K	270.0	278.9425	275.2129	271.4018	267.6442	263.7714	259.775	255.645	251.4472	247.2828
323K	190.6	212.5858	210.6866	208.7989	206.9292	205.022	203.0806	201.1065	199.0876	197.0282
333K	134.3	166.4602	165.4683	164.4753	163.4964	162.5171	161.5328	160.5376	159.5284	158.508

Table 4.10 Time to reach 63.2% of the equilibrium loading for CART Diffusion Simulation

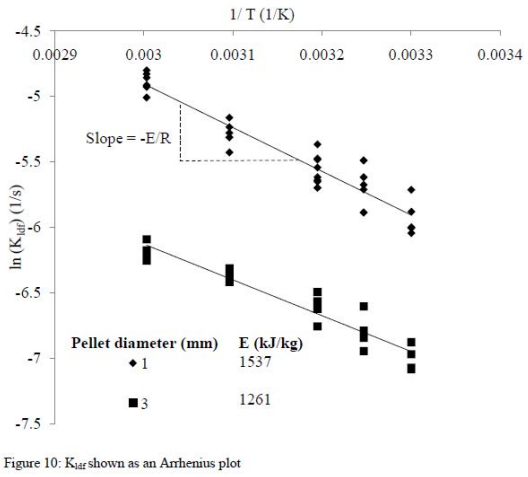

Figure 10: K_{ldf} shown as an Arrhenius plot

Figure 4.18 Arrhenius plot (Ahamat and Tierney [1]).

Figure 4.19 show the loading of the pellet for at two different times as obtained from the Diffusion model, the results were obtained from the simulation at an adsorbent temperature of 303K and an

evaporator pressure of 3000Pa. The figure shows the progressive diffusion of the sorbate into the pellet with time.

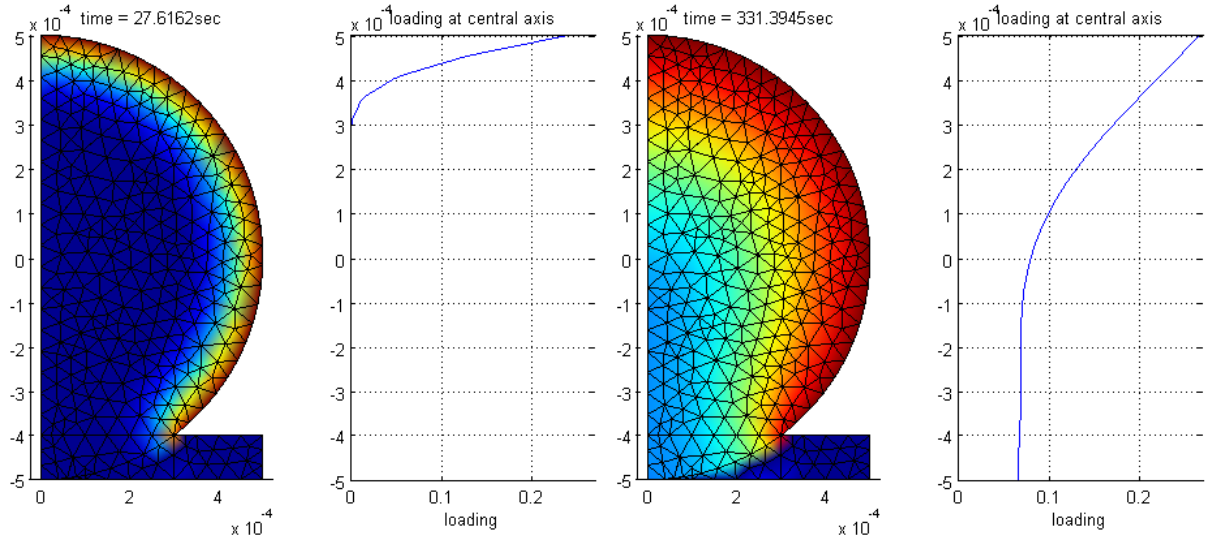

(a) (b)

Figure 4.19 Plots showing diffusion of sorbate into pellet at different instances in time. (a) at time = 27.6162 sec (b) at time = 331.3945 sec

The temperature distribution of over the pellet can also be plotted at different instances in time, this is shown in Figure 4.20. When this plot of temperatures is compared with the plot of diffusivity in the pellet (Figure 4.21), it shows that the variation of the diffusivity values is in agreement with the temperature, as the highest values of diffusivity occurs where the highest temperatures occur. The variation of temperature gradient with time is also in agreement with the variation of diffusivity gradient with time.

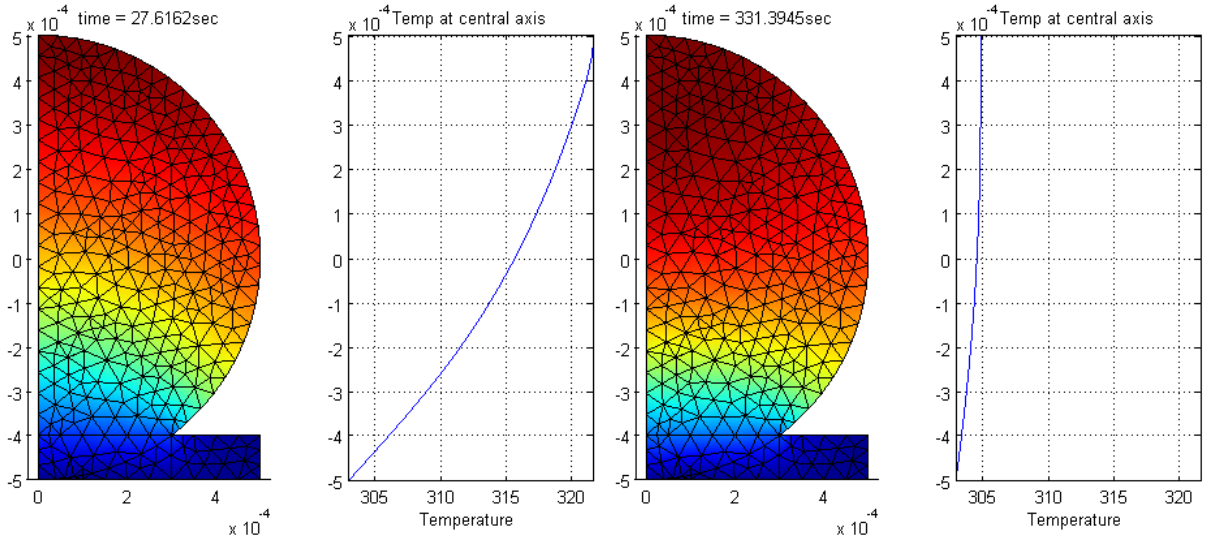

(a) (b)

Figure 4.20 Plots showing temperature gradient of pellet at different instances in time (a) at time = 27.6162 sec (b) at time = 331.3945 sec

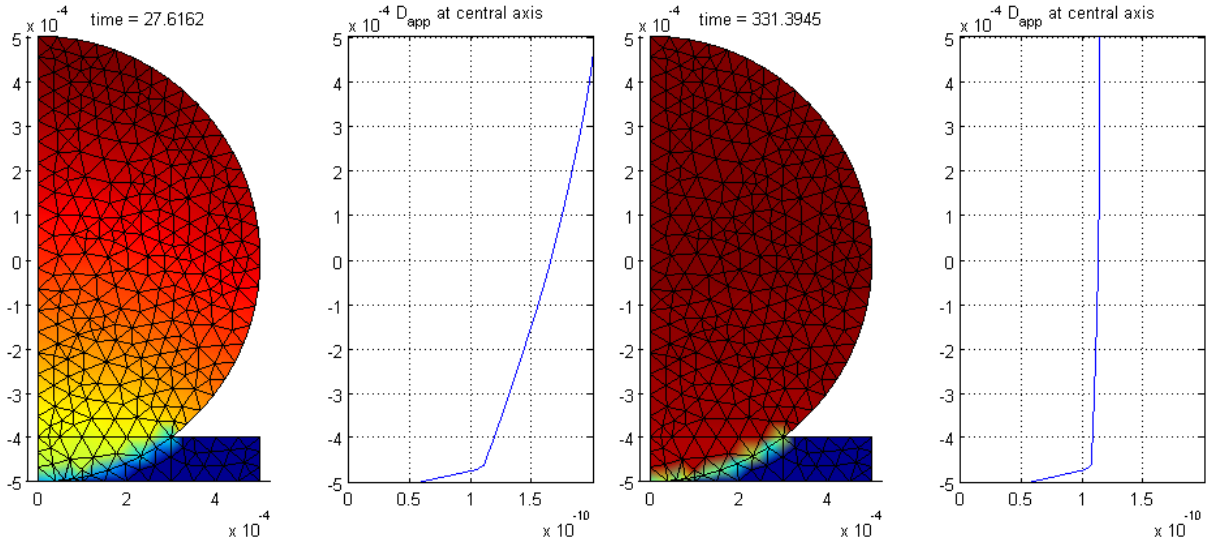

(a) (b)

Figure 4.21 Plots showing diffusivity of pellet at different instances in time.
(a) at time = 27.6162 sec (b) at time = 331.3945 sec

From the results in Figures 4.16 & 4.17, the LDF simulation result obtained from the PDE Toolbox and the AXI Routines are in close approximation, while the result obtained from the diffusion model shows a significant variation in comparison to the LDF model.

A similar variation between the two models has been reported by Raymond and Garimella [20] and also El-Sharkawy [19], these are shown in Figure 4.22. Although these models were carried out for spherical coordinates, the LDF model was observed to under-predict the loading at short adsorption times and to over-predict it at long adsorption times.

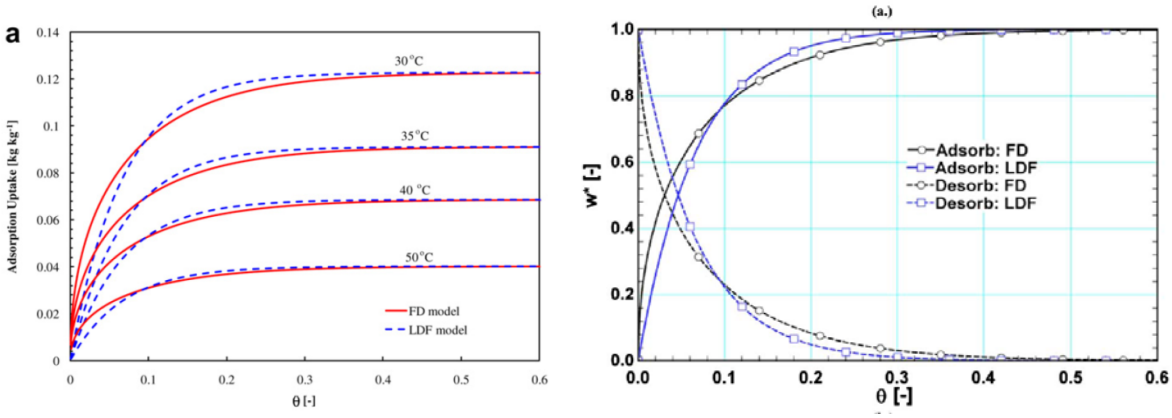

(a) (b)

Figure 4.22 Similar variations between LDF and Diffusion model obtained from models by
(a) El-sharkawy [19] (b) Raymond and Garimella [20]

CHAPTER 5 TESTS, RESULTS AND DISCUSSION

In this section several tests would be set up to investigate the effect of the following conditions on the adsorption process; that is the adsorption kinetics and the temperature gradient in the pellet. The effect of the varying conditions on the adsorption kinetics would be considered at the time taken to attain 63.2% of the equilibrium loading values, as it would be uneconomical to allow the cycle continue until the pellet is fully loaded. 63.2% of the pellet loading occurs after one time constant, while 86.5% occurs after a period equal to two time constants. For most practical cases it would be more economical to stop the adsorption process after one or two time constants as additional loading after this stage is marginal.

The conditions to be investigated are outlined below:

- Bond thickness
- Thermal conductivity of the pellet
- Bond and pellet density
- Adsorbent (or pellet) temperature
- Evaporator pressure

5.1 Tests

The test would be setup as shown below and the parameters to be investigated would then be varied, while other parameters are kept constant. The result obtained would then be studied to determine if these parameters affect the adsorption process; and if they do, what these effects are.

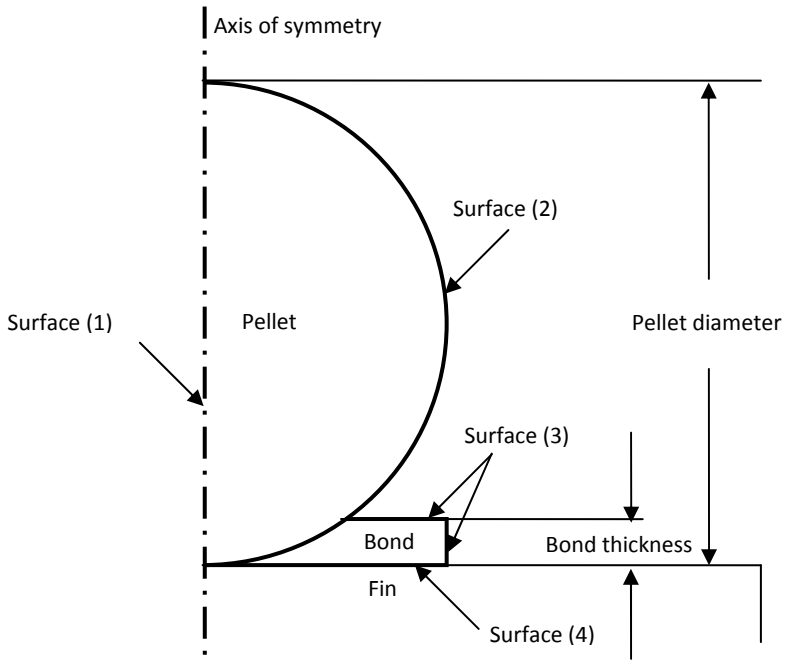

Figure 5.1 Model geometry and different surfaces (or boundaries)

The base values of all parameters used in the simulations are shown in Table 5.1 , these values are then varied as required in each of the simulations carried out. The fin temperature is mostly referred to as the adsorbent temperature.

Property (Unit)	Value[1]
Silica gel type	Type A
Thermal conductivity of pellet (W/mK)	0.174
Thermal conductivity of bond (W/mK)	0.2
Density of pellet (kg/m^3)	1306
Density of bond (kg/m^3)	1200
Heat capacity of pellet (J/kgK)	921
Heat capacity of bond (J/kgK)	1000
Heat transfer coefficient of pellet (W/m^{2}K)	0
Heat transfer coefficient of bond (W/m^{2}K)	0
Radius of pellet (m)	5.00E-04
Thickness of bond (m)	0.0001
Heat of adsorption (J/kg)	2.69E+06
Activation energy (J/mol)	4.20E+04
Fin temperature (K)	313
Ambient temperature (K)	297.0978
Initial temperature (K)	313
Geometric factor	15
Surface diffusivity at zero loading	2.54E-04
Molar gas constant (J/mol)	8.3145
Molar mass of adsorbate (kg/kmol)	18
Henry's constant at zero loading(Pa^{-1})	5.9E-13
Monolayer adsorption capacity (kg/kg)	0.4
Toth parameter	12

Table 5.1 Base parameters used for simulations

5.1.1 Effect of Bond Thickness

This test was carried out to investigate the effect of varying bond thickness on the adsorption process that takes place in the adsorbent. The test was simulated using parameters similar to those used in the experiment carried out by Ahamat and Tierney [1], but in this case the test was simulated using various bond thicknesses. The bond thickness was then varied between the value 0.02mm and 0.2mm The results for the simulation are shown in Figures 5.2 & 5.3.

From the obtained simulation results it was observed that variation in bond thickness affected both the temperature and the loading of the pellet.

At short adsorption times the mean pellet temperature was observed to drop as the bond thickness was increased, this is shown in Figure 5.3 This effect can be attributed to the fact that an increased bond thickness provides a larger contact area between the bond and the pellet. This larger contact area allows heat to be transmitted away from the pellet faster, than with a small bond thickness. This is illustrated in Figure 5.4.

The mean pellet loading was also observed to be affected by the bond thickness. Two different trends were observed for the LDF and the Diffusion models as shown in Figure 5.2(d). In the LDF model, the loading rate was observed to increase with increasing bond thickness, while in the Diffusion model, the loading rate was observed to decrease with increasing bond thickness. These two trends are can be verified by the plot of time constant against bond thickness for both the LDF and Diffusion models (Figure 5.2(d)).

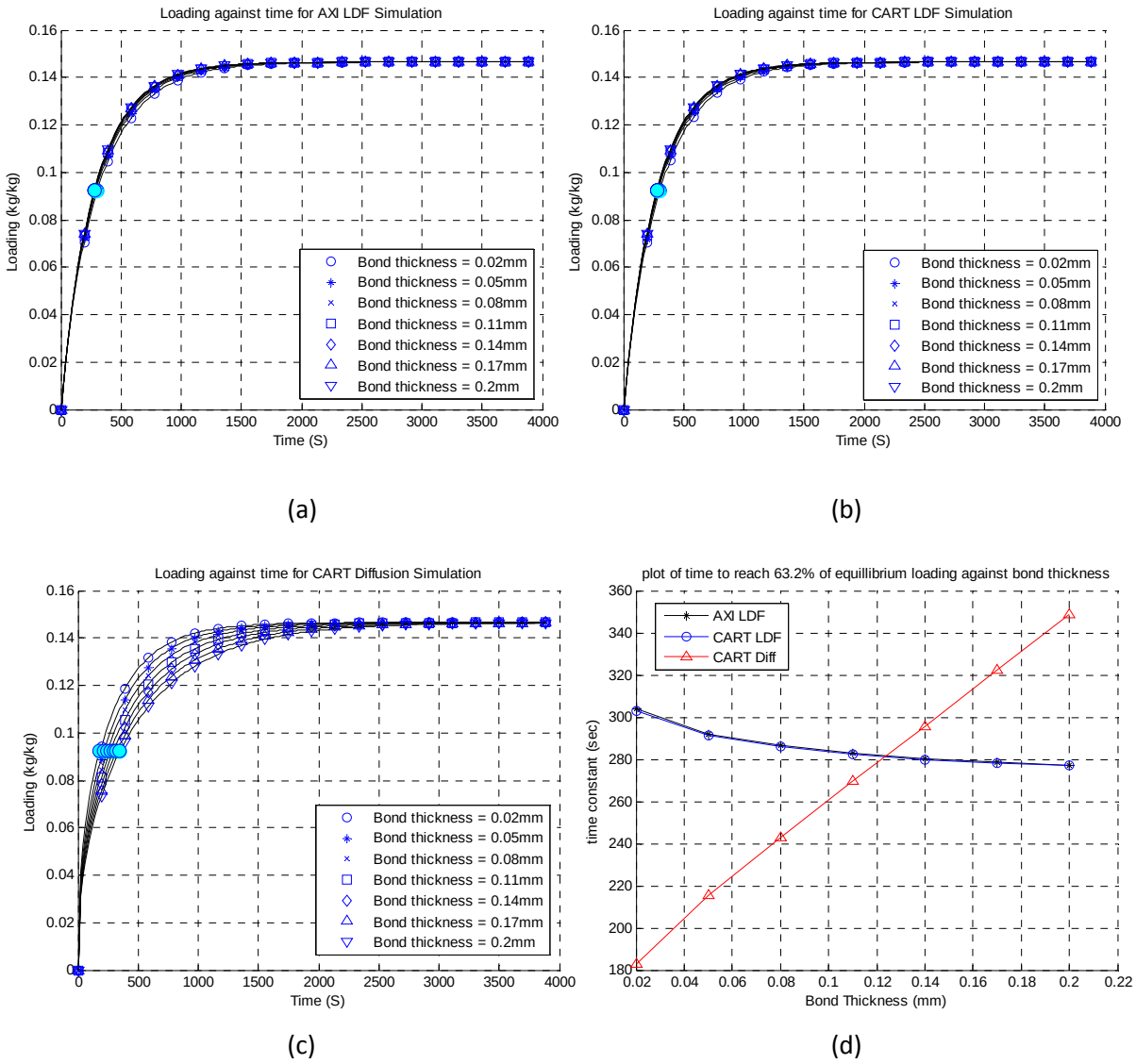

Figure 5.2 Plot of loading against time and time constant for different bond thicknesses (a)For AXI LDF simulation (b) For CART LDF simulation (c) For CART Diffusion simulation (d) Plot of time-constant against bond thickness for the 3 models

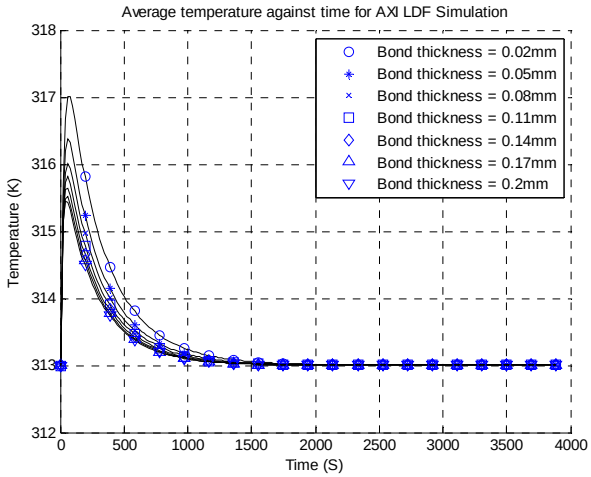

(a)

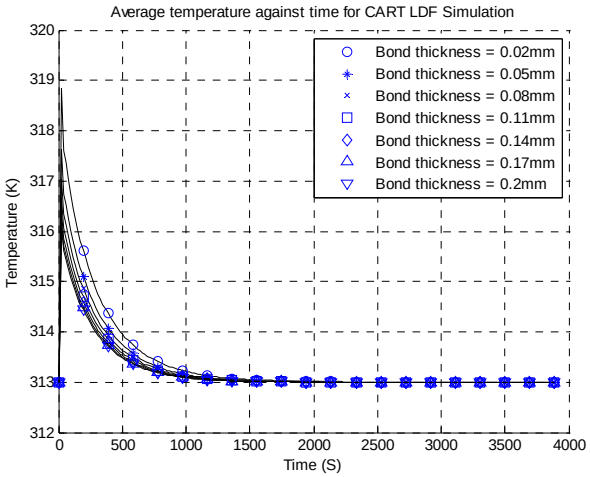

(b)

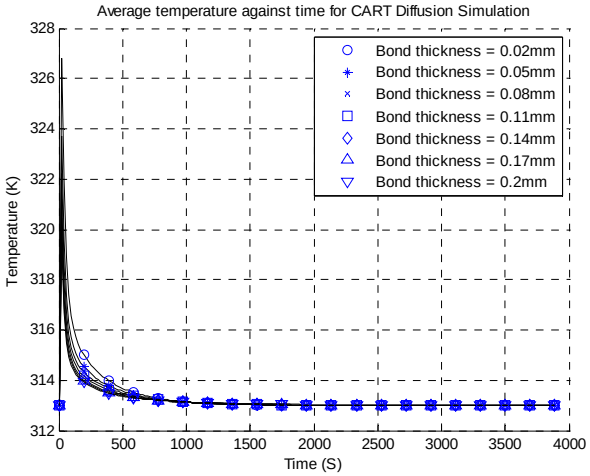

(c)

Figure 5.3 Plots of temperature against time
(a)For AXI LDF simulation (b) For CART LDF simulation (c) For CART Diffusion simulation

In the plot for the LDF model the time constant decreased with increasing bond thickness, suggesting a faster loading rate. This effect is due to the fact that the pellet gets cooled down faster with increasing bond thicknesses, thereby increasing the equilibrium adsorption capacity of the pellet as given by the Toth isotherm. An increase in equilibrium adsorption capacity (X^*) invariably increases the driving force (or rate of adsorption) as given by the LDF equation (equation 3.8) or diffusion equation (equation 3.12).

Another effect of reduced temperature is that of reduced diffusivity, lower temperatures result in lower diffusivity values, but because the temperature used to calculate the diffusivity value in the LDF model is the average pellet temperature, the effect of temperature on diffusivity is not so pronounced.

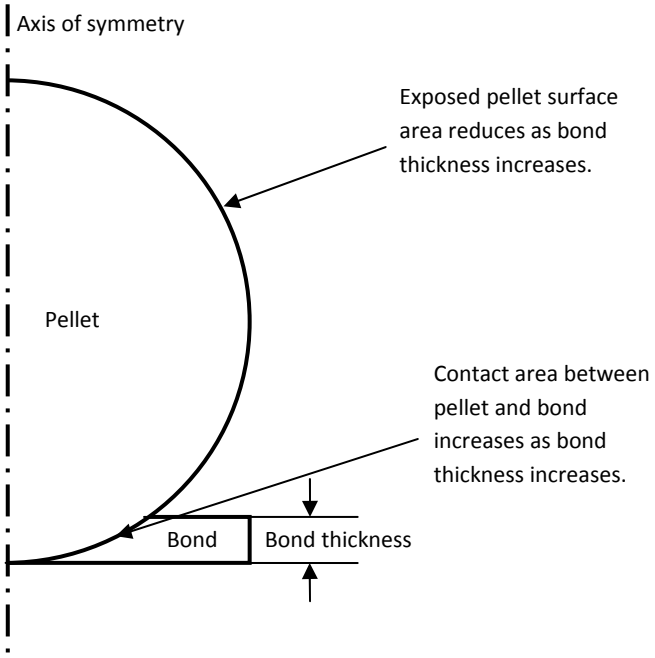

Figure 5.4 Model geometry showing effect of increased bond thickness

The average pellet temperature at a time of 252.6298 sec for the LDF simulation with the thicker bond shown in Figure 5.5 is 314.1604K, while that for the thinner bond is 315.1365K. This implies that the average pellet temperature decreased by 1K when the bond thickness was increased from 0.02mm to 0.2mm, and the corresponding reduction in time constant was about 27 seconds (as shown in Figure 5.2(d)).

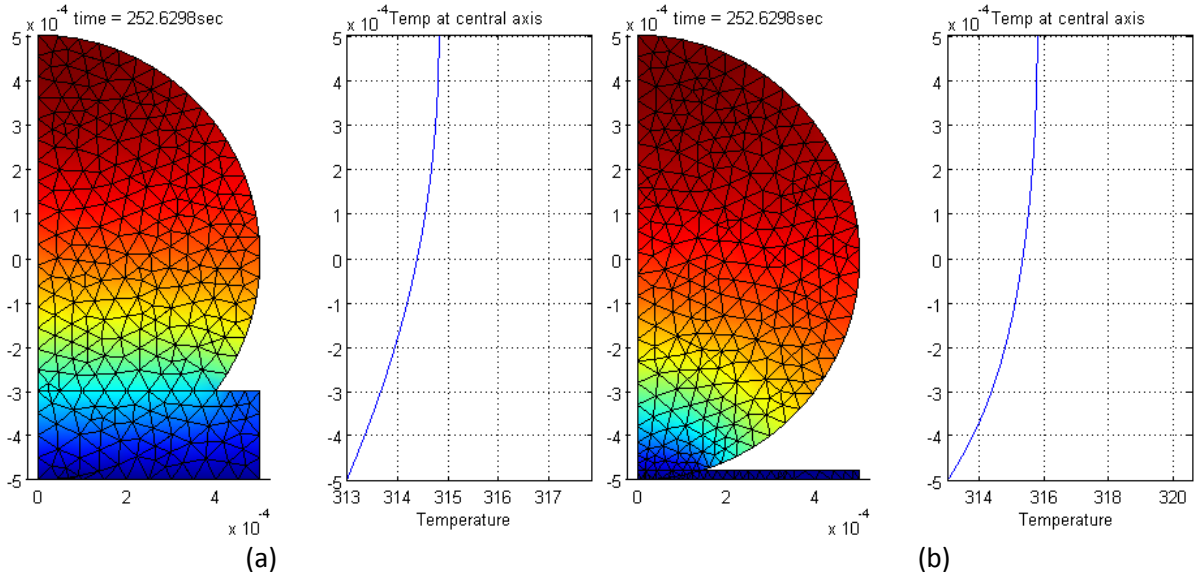

Figure 5.5 LDF model showing slight temperature differences for different bond thickness (a) For bond thickness = 0.2mm (b) For bond thickness = 0.02mm

On the other hand, the time constant for the Diffusion model increased with increasing bond thickness. This effect seems unusual, as the pellet gets cooled faster due to an increased pellet-bond contact area. But unlike the LDF model, the diffusion model depends on the exposed surface area of

the pellet for adsorption to take place, the larger the exposed surface area the faster the diffusion process. A larger bond thickness results in a reduced external surface area for the pellet, this in effect slows down the adsorption process, this is illustrated in Figure 5.4.

The plot of temperature gradient for the diffusion model Figure 5.6, shows a slight difference in the temperature gradient for two different pellet thickness. The difference in temperature gradients observed is about 1K, similar to that observed for the LDF model.

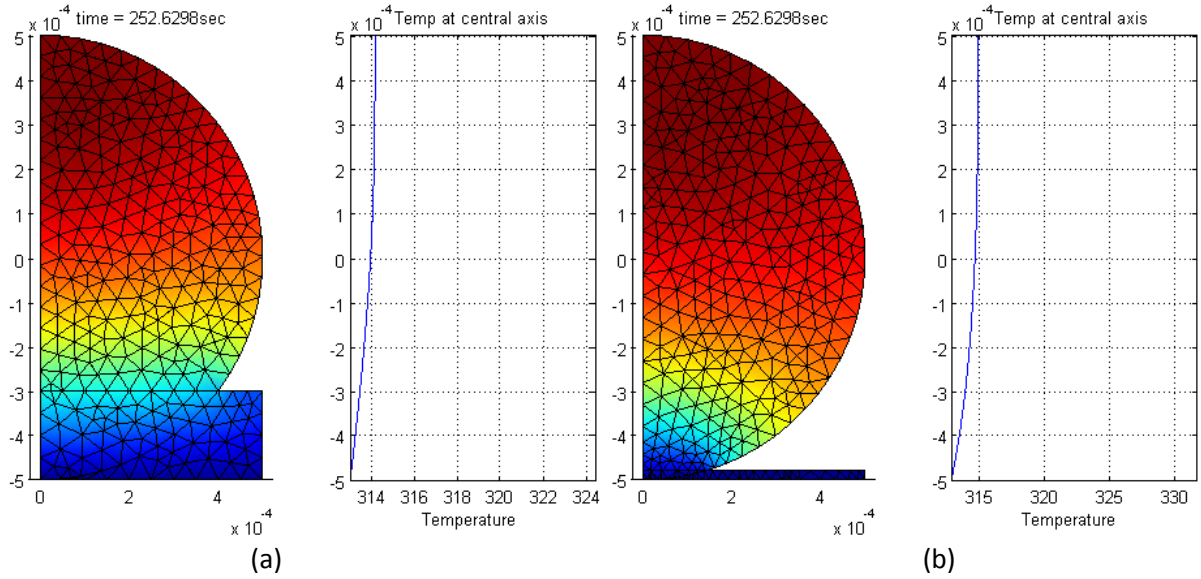

Figure 5.6 Diffusion model showing slight temperature differences for different bond thickness (a) For bond thickness = 0.2mm (b) For bond thickness = 0.02mm

The major difference in loading resulted from the exposed surface area for adsorption, this is shown in Figure 5.7, the larger exposed surface area for adsorption in the simulation with a smaller bond thickness resulted in higher pellet loading at the same time instant, than the loading in the simulation with a larger bond thickness.

In the case of the diffusion model, the average pellet temperature observed at a time of 252.6298 seconds was 313.7438K for the simulation with a thicker bond while that for the thinner bond was 314.6057K showing a difference in temperature of approximately 1K, but due to the surface area effect explained above the reduction in time constant when the bond thickness was increased was about 170 seconds, as opposed to the 27 seconds observed in the LDF model.

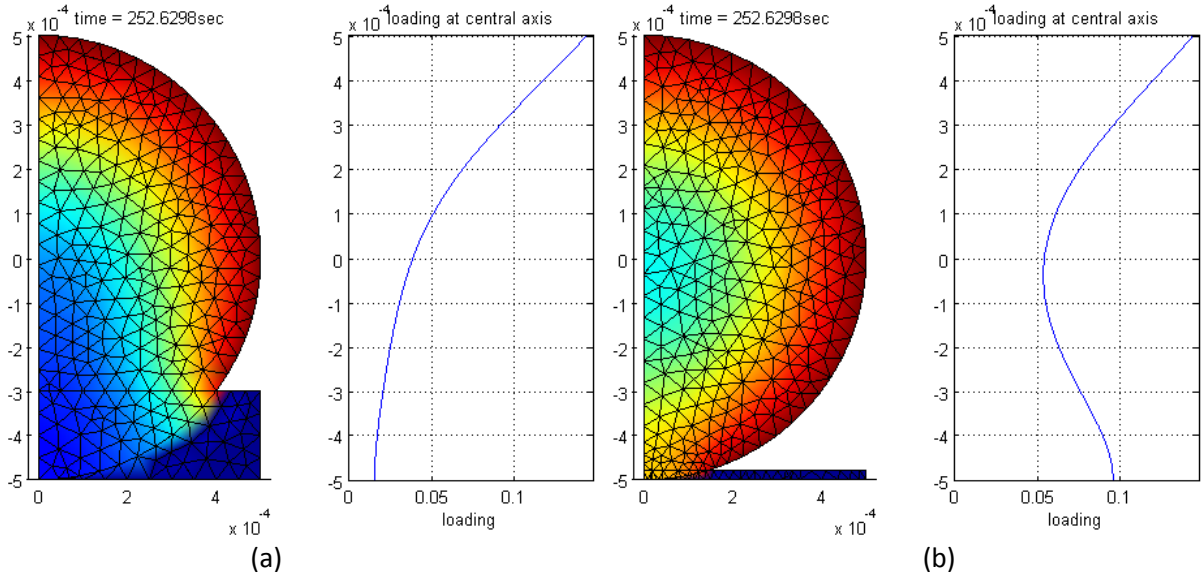

Figure 5.7 Diffusion model showing differences in loading for different bond thickness (a) For bond thickness = 0.2mm (b) For bond thickness = 0.02mm

5.1.2 Effect of Thermal Conductivity of Pellet

This test was carried out to investigate the effect of varying thermal conductivity of the pellet on the adsorption process, that takes place in the adsorbent. The test was simulated using parameters similar to those used in the experiment carried out by Ahamat and Tierney [1]. The values of the base parameters used for this simulation is similar to those used for the test on varying bond thickness and is shown in Table 5.1. In this case the thermal conductivity of the pellet was varied between the values of 0.1W/mK and 1.5W/mK.

Increased thermal conductivity brings about faster cooling of the pellet, as the heat generated by the adsorption process is transferred away from the pellet faster as the thermal conductivity increases. Therefore increase in thermal conductivity results in a reduction in the average pellet temperature of the pellet (when all other conditions remain the same), this effect is observed in Figure5.9.

The variation in the loading kinetics of the pellet also exhibits a contrasting trend for the LDF and Diffusion models. The time constant for the LDF model decreases with increasing pellet thermal conductivity while that for the Diffusion model increases with an increase in pellet thermal conductivity.

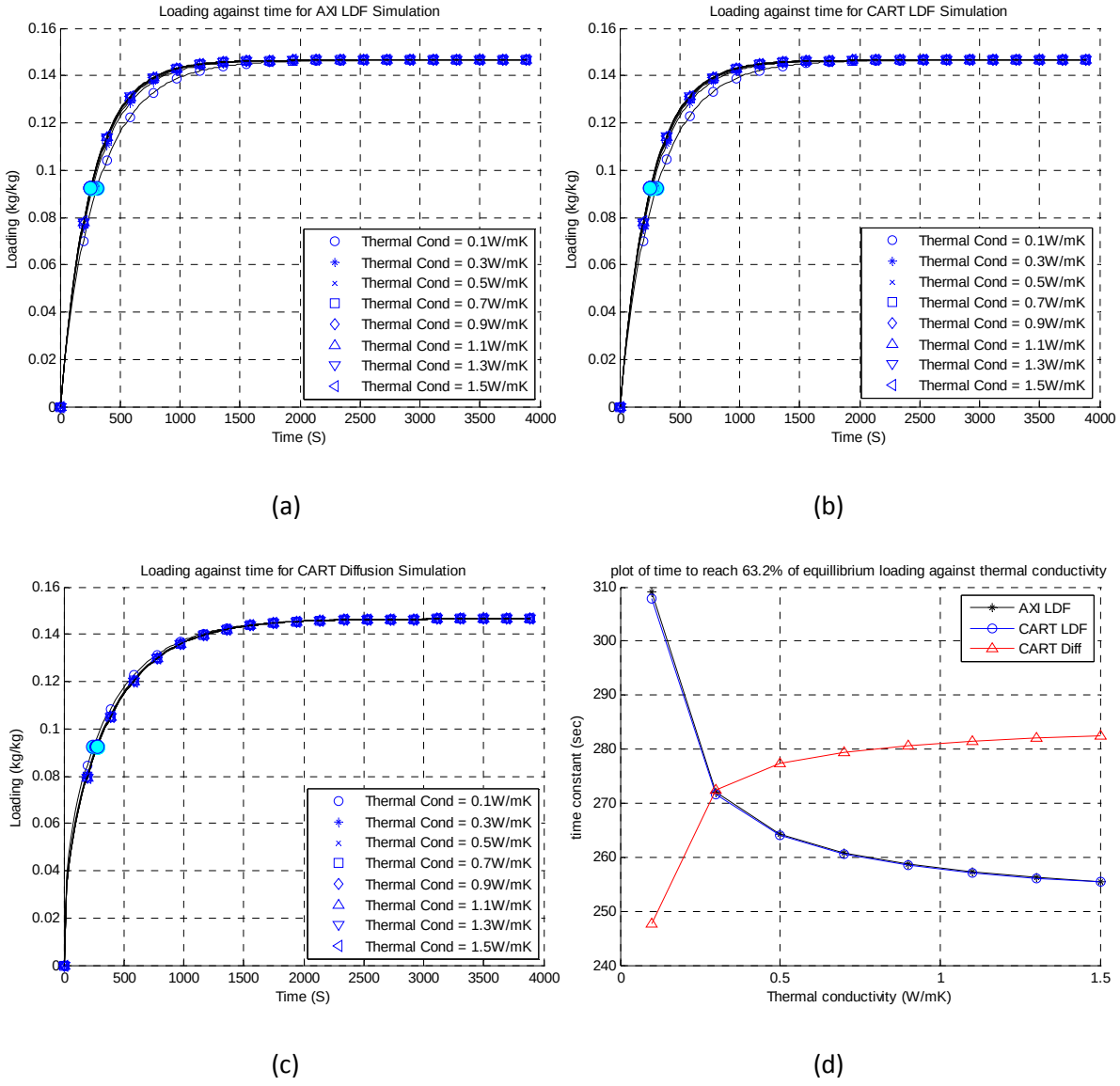

Figure 5.8 Plot of loading against time and time constant for different pellet thermal conductivities
(a)For AXI LDF simulation (b) For CART LDF simulation (c) For CART Diffusion simulation (d) Plot of time-constant against bond thickness for the 3 models

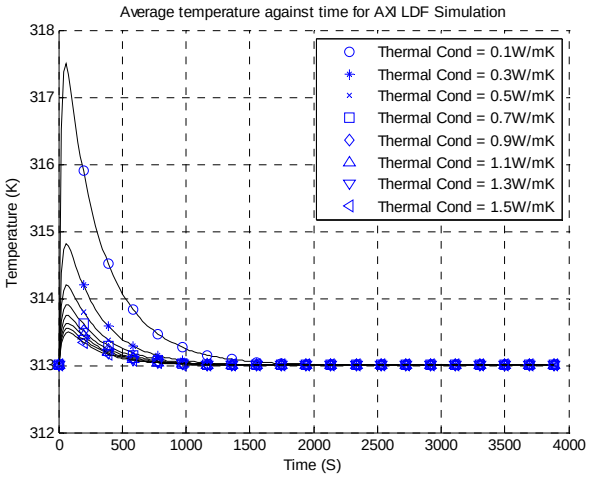

(a)

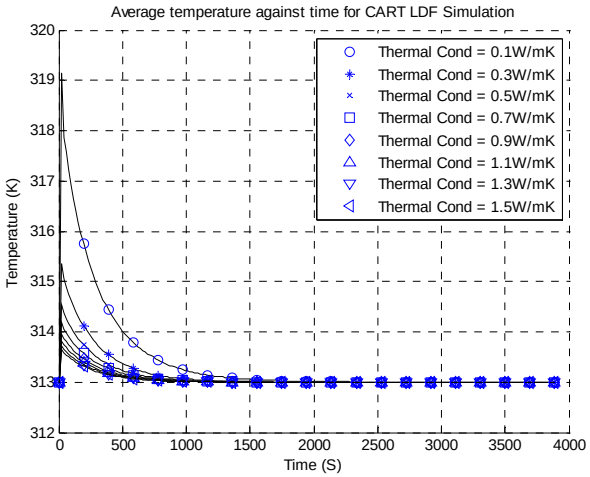

(b)

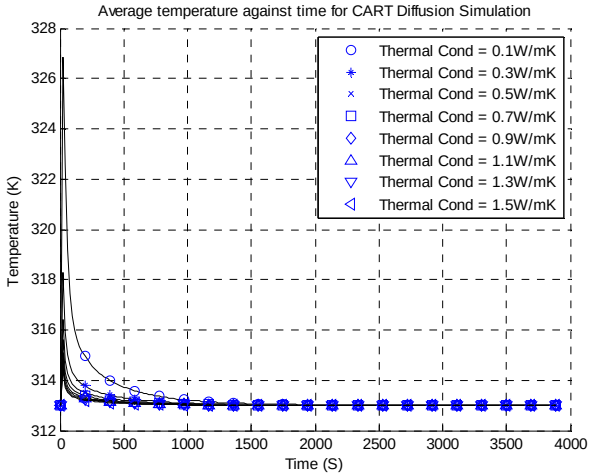

(c)

Figure 5.9 Plots of temperature against time
(a)For AXI LDF simulation (b) For CART LDF simulation (c) For CART Diffusion simulation

The faster adsorption rate experienced at higher thermal conductivity values for the LDF model is due to the increased loading capacity at lower temperatures. The diffusivity is also somewhat reduced at lower temperatures. It is important to note that the temperature which is used in computing the value of the diffusivity and equilibrium loading capacity for the LDF model is the mean pellet temperature. The time constant of the LDF model reduced by about 40 seconds when the thermal conductivity was increased from a value of 0.3W/mK to 1.5W/mK.

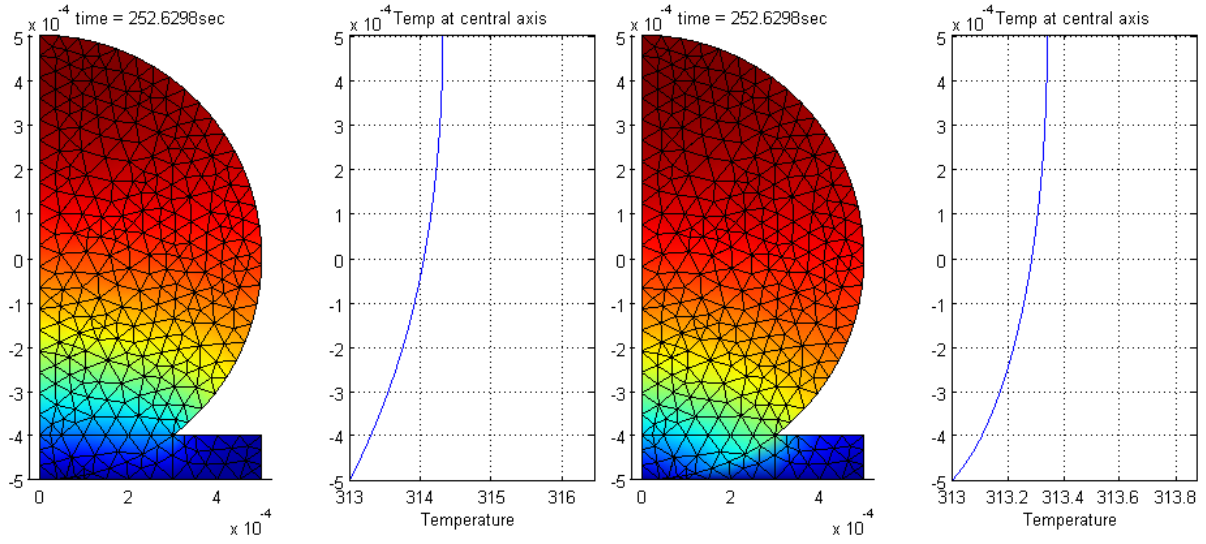

(a) (b)

Figure 5.10 Plots showing temperature differences for different pellet thermal conductivity in the LDF model
(a) For thermal conductivity = 0.1W/mK (b) For bond thickness = 1.5W/mK

The Diffusion model showed a slower rate of adsorption as the thermal conductivity increased, this can be linked to the reduced temperature in the pellet and the reduced diffusivity. This suggests that the effect of the reduced diffusivity dominates the increased equilibrium loading capacity.

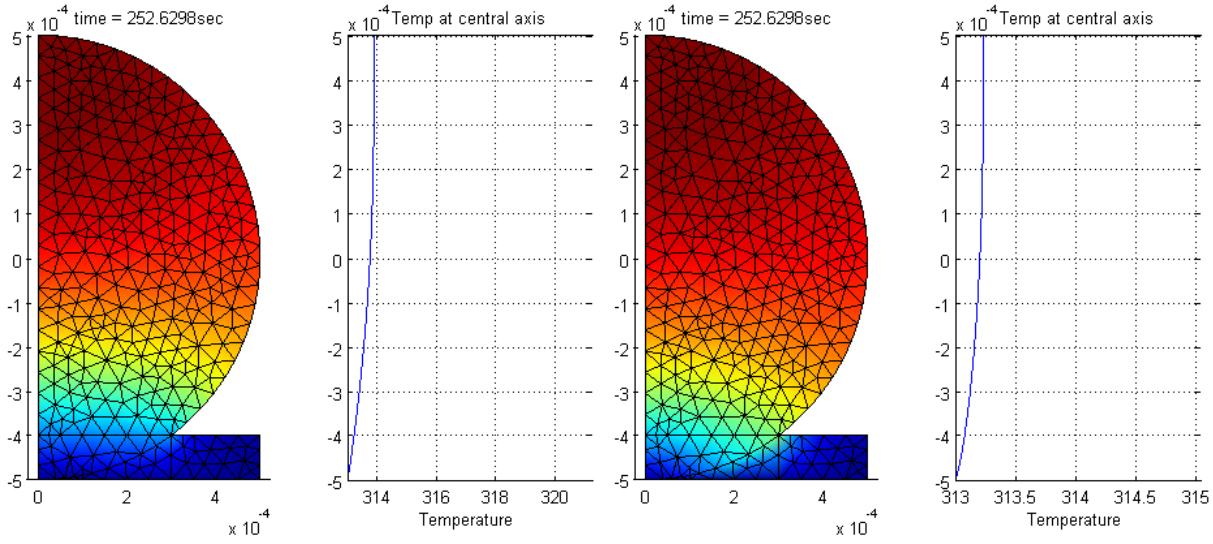

(a) (b)

Figure 5.11 Plots showing temperature differences for different pellet thermal conductivities in the Diffusion model
(a) For thermal conductivity = 0.1W/mK (b) For bond thickness = 1.5W/mK

5.1.3 Effect of Pellet Density

This test was carried out to investigate the effect of varying pellet density on the adsorption process that takes place in the adsorbent. The test was simulated using parameters similar to those used in the experiment carried out by Ahamat and Tierney [1]. The values of the base parameters used for this simulation is shown in Table 5.1. In this case the pellet density was varied between the values of 600 kg/m^3 and 2200 kg/m^3.

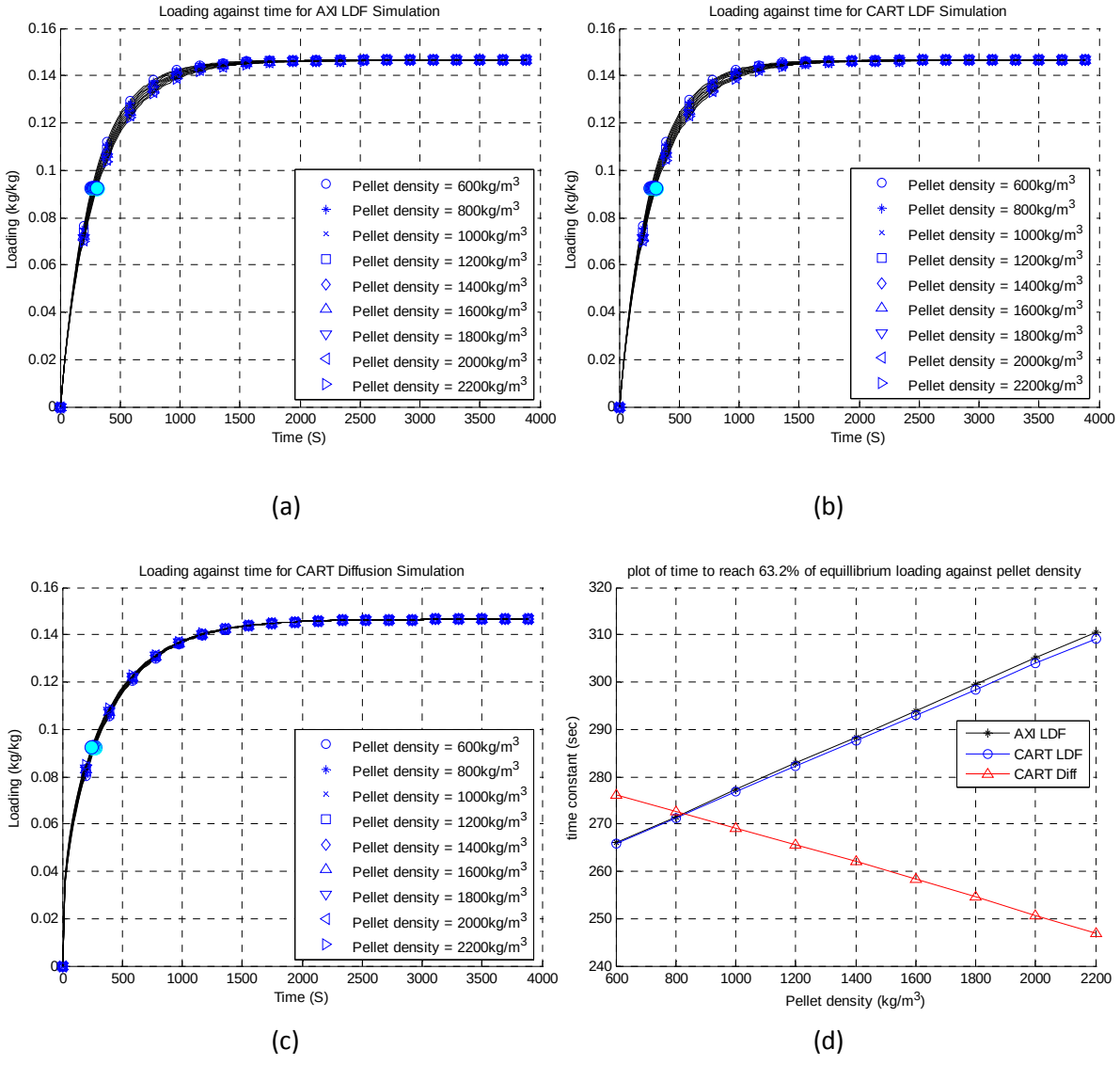

Figure 5.12 Plot of loading against time and time constant for different pellet densities (a)For AXI LDF simulation (b) For CART LDF simulation (c) For CART Diffusion simulation (d) Plot of time-constant against pellet densities for the 3 models

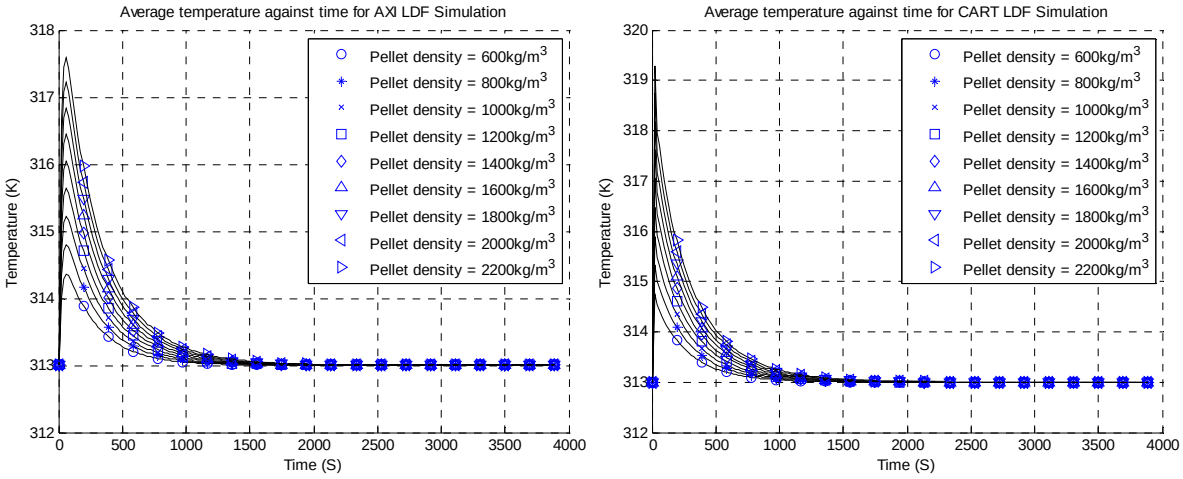

(a) (b)

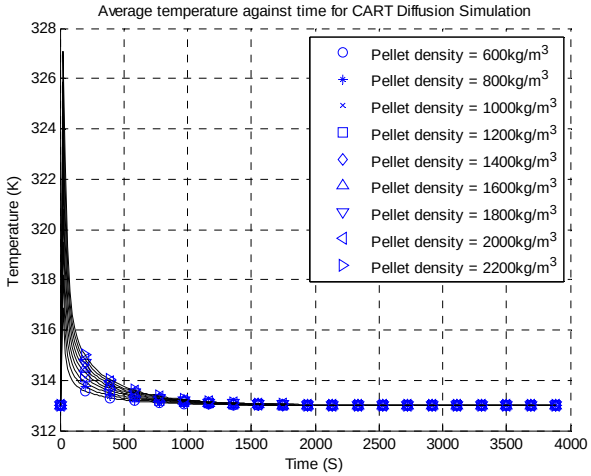

(c)

Figure 5.13 Plot of average pellet temperature against time
(a)For AXI LDF simulation (b) For CART LDF simulation (c) For CART Diffusion simulation

A higher density increases the heat storage capacity of the pellet, and reduces the cooling rate, thereby resulting in higher temperatures being sustained in the pellet for a longer time as can be observed in Figure 5.13 The same phenomenon similar to what was observed in previous tests, was observed here also. An increase in temperature leads to a faster rate of adsorption in the Diffusion model, while an increase in temperature leads to a slower rate of adsorption in the LDF model.

$$\rho c_p \frac{\partial T}{\partial t} = k\nabla^2 T + Q\rho D_{app}^{surf} \nabla^2 X \quad \therefore \quad c_p \frac{\partial T}{\partial t} = \frac{k}{\rho}\nabla^2 T + Q D_{app}^{surf} \nabla^2 X$$

$\frac{\partial T}{\partial t} \propto \frac{1}{\rho}$ $\Rightarrow$ a higher density results in lower rate of change of temperature, therefore the pellet retains high temperatures for longer periods.

5.1.4 Effect of Initial Adsorbent Temperature and Fin Temperature

This test was carried out to investigate the effect of varying the adsorbent temperature on the adsorption process that takes place in the adsorbent. The test was simulated using parameters similar to those used in the experiment carried out by Ahamat and Tierney. The values of the base parameters used for this simulation are shown in Table 5.1 In this case adsorbent temperature of the pellet was varied between the values of 303K and 333K.

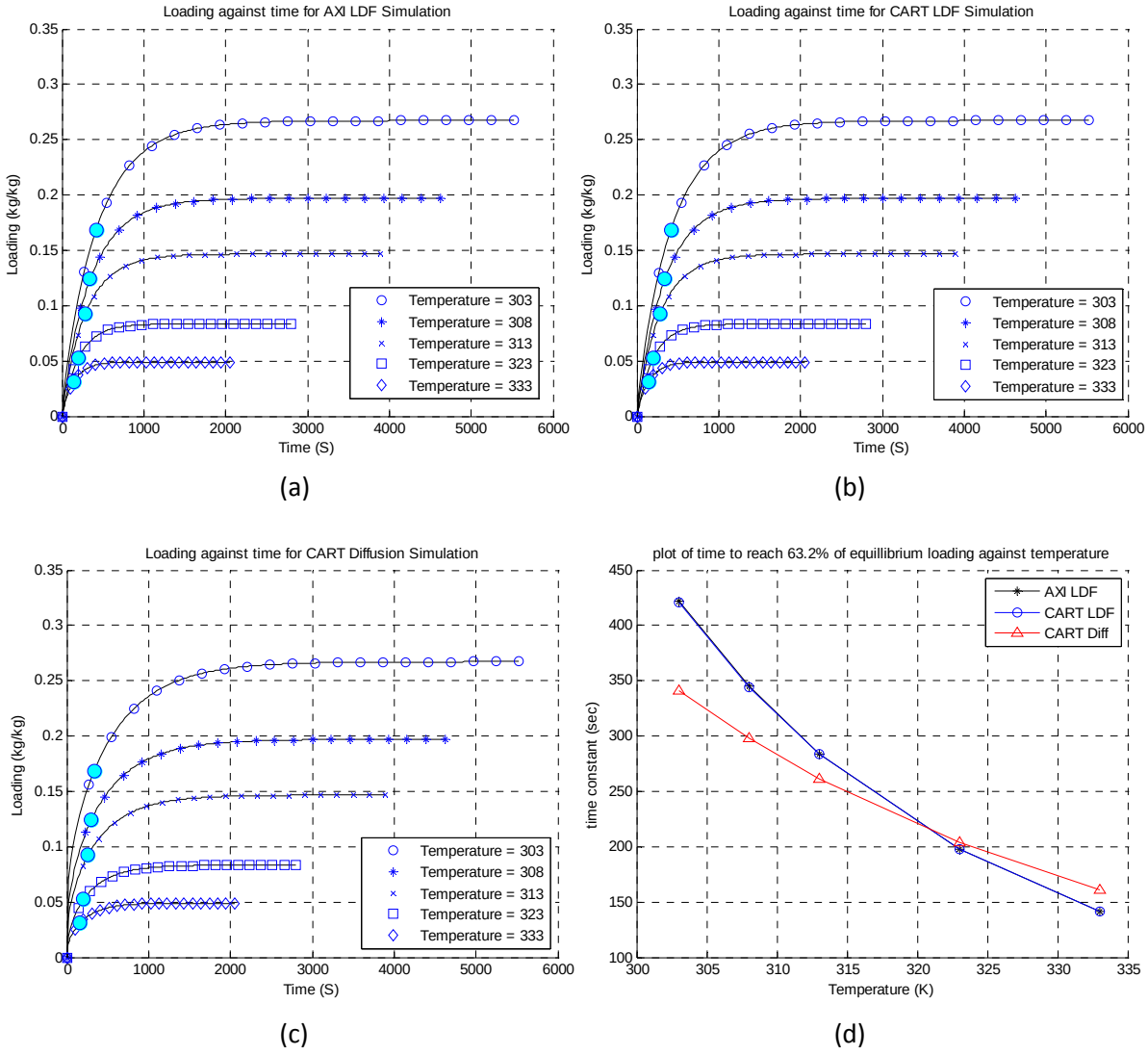

Figure 5.14 Plot of loading against time and time constant for different adsorbent temperatures (a)For AXI LDF simulation (b) For CART LDF simulation (c) For CART Diffusion simulation (d) Plot of time-constant against adsorbent temperature for the 3 models

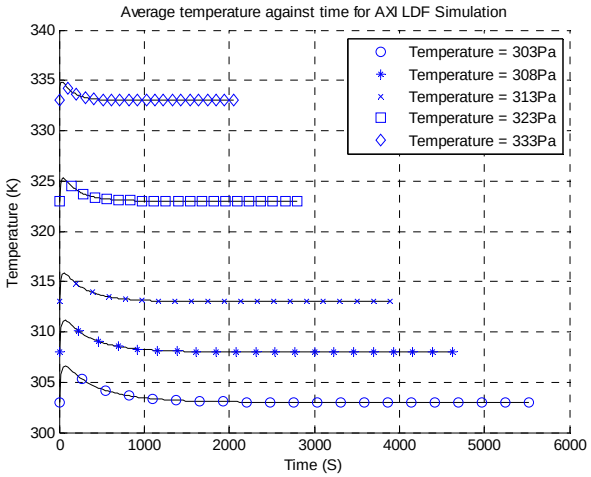

(a)

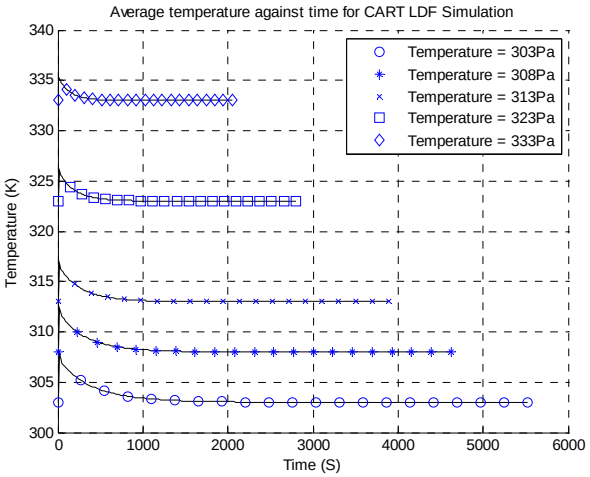

(b)

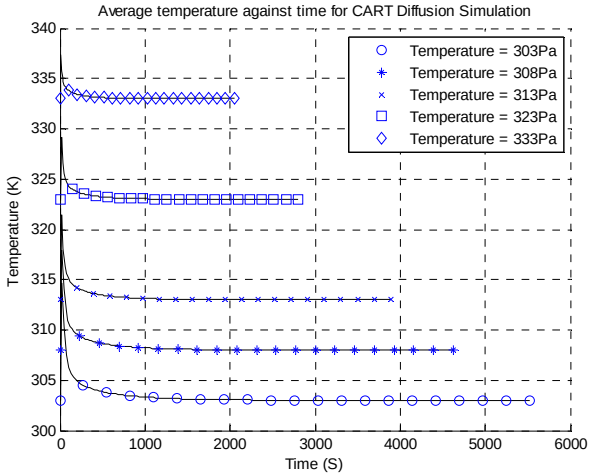

(c)

Figure 5.15 Plots of temperature against time
(a)For AXI LDF simulation (b) For CART LDF simulation (c) For CART Diffusion simulation

An increase in sorbent temperature resulted in a decrease in the time constant (implying a faster adsorption rate) regardless of the model employed.

This can be attributed entirely to an increase in diffusivity with increased temperature. The increase in temperatures here is a little different from what was observed in the previous simulations, because in this case the increased temperature is sustained over the entire period of adsorption and occurs over the entire pellet, as opposed to the localized temperature variations which occur at short adsorption times in the other simulations. The effect of this sustained global change in temperature is the marked difference in rates of adsorption.

5.1.5 Effect of Evaporator Pressure

This test was carried out to investigate the effect of varying the evaporator pressure on the adsorption process that takes place in the adsorbent. The test was simulated using parameters similar to those used in the experiment carried out by Ahamat and Tierney [1]. The base values used in this simulation is given in Table5.1. The evaporator pressure was varied between 1000Pa and 5000Pa.

The results obtained from the simulation are shown in the Figures 5.16 and 5.17. The plots show the average pellet loading against time with a cyan coloured circle indicating the point of 63.2% loading. A plot of time constant (i.e. time to reach 63.2% loading) against pressure is also shown for the different models employed.

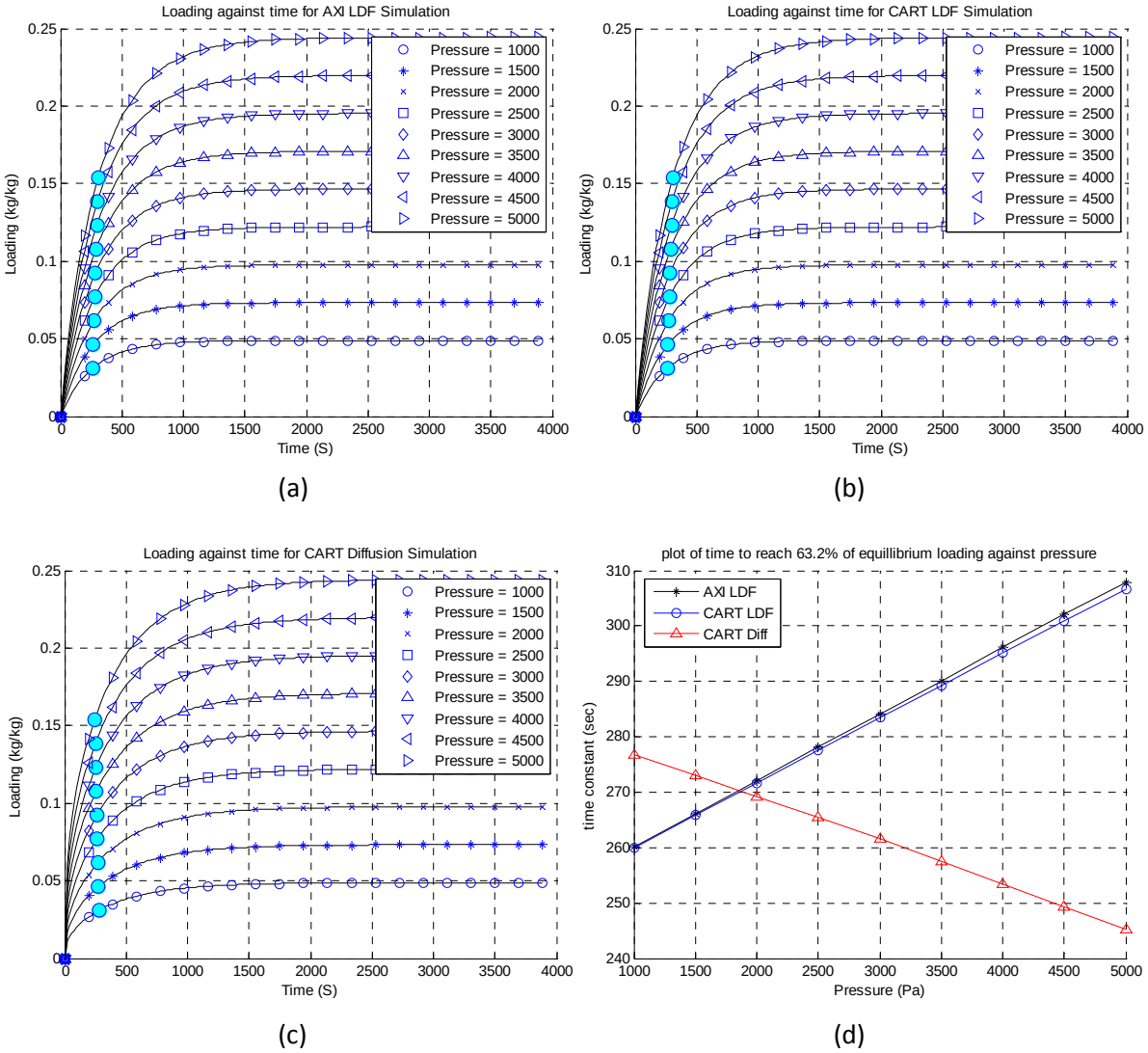

Figure 5.16 Plot of loading against time and time constant for different evaporator pressures (a)For AXI LDF simulation (b) For CART LDF simulation (c) For CART Diffusion simulation (d) Plot of time-constant against evaporator pressure for the 3 models

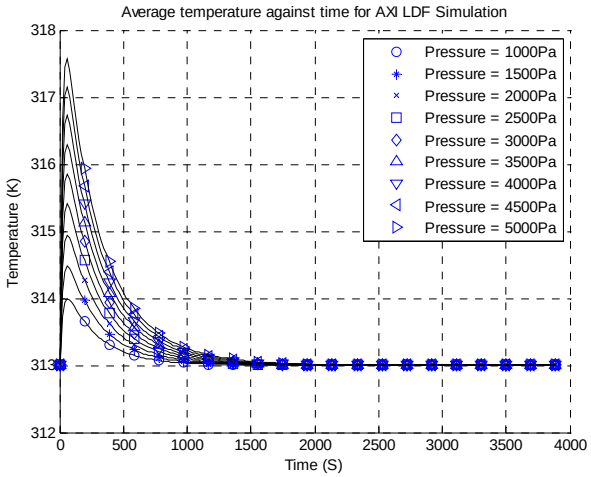

(a)

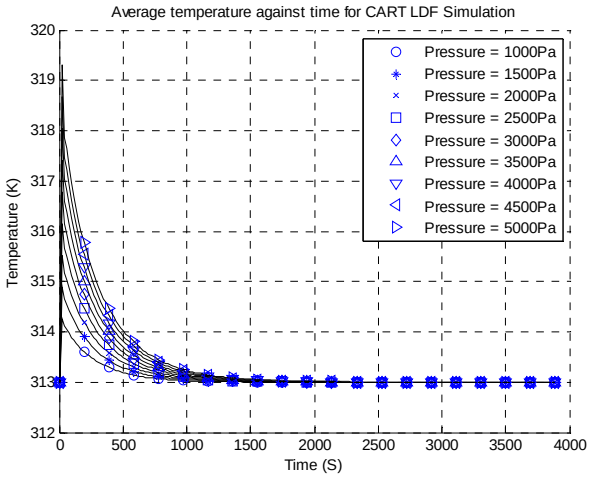

(b)

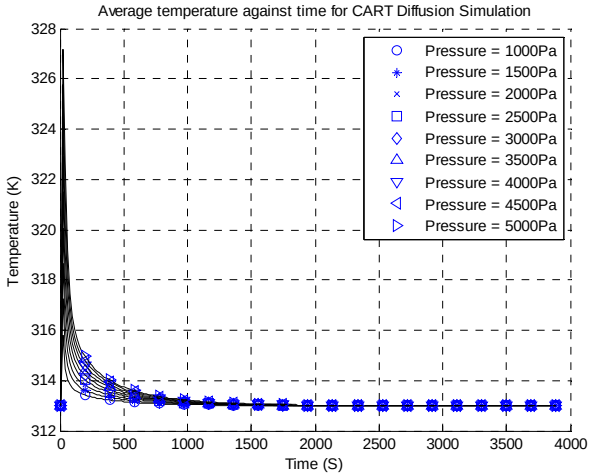

(c)

Figure 5.17 Plots of temperature against time
(a)For AXI LDF simulation (b) For CART LDF simulation (c) For CART Diffusion simulation

From the plots of mean temperature against time it was observed that; the mean pellet temperatures at short adsorption times was greater for higher evaporator pressures.

As discussed in previous tests, higher temperatures brings about two opposing effects on the rate of adsorption; that of an increased diffusivity and that of a reduced loading capacity. From the results obtained from this simulation it was observed that the rate of adsorption increased with increasing temperature for the diffusion model while it decreased with increasing temperature for the LDF model. This observation suggests that the rate of adsorption in the diffusion model is dominated by the effect of diffusivity while that of the LDF model is dominated by the effect of loading capacity.

A research carried out by Clarkson and Bustin[35] in which they studied the adsorption of methane (CH_4) and (CO_2) on coal showed that the effective adsorption diffusivity increases with pressure. which is similar to what was observed for the diffusion model

5.2 General Discussion

From the simulations carried out it was observed that; for all "adsorbent temperatures" the average pellet temperature is not constant throughout the adsorption process, but the pellet experiences temperature changes which could be as high as 5K for LDF model and 10K for the diffusion model. Although these high temperatures are not sustained for a long period of time, they occur during the period when most of the adsorption takes place, therefore they can have a substantial effect on the rate of adsorption.

Apart from the average pellet temperature changes over time, temperature gradients also exist across the pellet at short adsorption times. The effect of these temperature gradients is what causes the differences observed between the LDF model and the diffusion model.

The LDF model does not take temperature gradients across the pellet into account, instead it averages it and uses this average to obtain a value of diffusivity and loading capacity. On the other hand the diffusion model takes these pellet temperature gradients into account, and determines a diffusivity value at each location in the pellet, based on the local temperature. The result is that, at short adsorption times, the higher temperatures are localized in the exterior portion of the pellet, which contains higher loading also, therefore the adsorption rate is much higher at this stage of the process

The opposing effects of equilibrium loading capacity and diffusivity, in which equilibrium loading capacity tends to decrease with increase in pellet temperature, while the diffusivity increases with an increase in pellet temperature, has counteracting effects on the adsorption kinetics. As the temperature of the pellet increases the equilibrium loading capacity of the pellet decreases, this tends to reduce the rate of adsorption, while on the other hand as the temperature increases the diffusivity increases this tends to increase the rate of adsorption. This effect is illustrated by the equations below and the explanation following it.

$$For\ the\ LDF\ model\ the\ rate\ of\ adsorption\ is\ \frac{dX}{dt} = K_{ldf}(X^* - X)$$

$$where\ K_{ldf} = f(D_{app})$$

$$For\ the\ diffusion\ model\ the\ rate\ of\ adsroption\ is\ \frac{\partial X}{\partial t} = D_{app}\nabla^2 X$$

$$where\ \nabla^2 X = f(X^*)$$

$$For\ both\ models\ it\ is\ obvious\ that\ the\ rate\ of\ adsroption\ \frac{\partial X}{\partial t} = f(X^*, D_{app})$$

$$X^* = f_1(Temp)\ \ where\ \ X^* \propto \frac{1}{Temp},$$

$$D_{app} = f_2(Temp)\ \ where\ \ D_{app} \propto Temp$$

$$Therefore\ \frac{dX}{dt} = f_1(Temp) \times f_2(Temp)$$

$$Where\ f_1(Temp)\ is\ the\ loading\ capacity\ effect\ of\ temperature$$

$$and\ f_2(Temp)\ is\ the\ diffusivity\ effect\ of\ temperature$$

The greater of these two effects dominates the rate of adsorption, in the diffusion model it was observed that the diffusivity effect dominated, while in the LDF model, the effect of loading capacity dominated.

From the studies carried out above, we can divide the types of temperature changes occurring in the adsorption process into two namely:

- Temporary temperature changes: these occur for a short time and takes place at the start of adsorption.
- Sustained temperature changes: these occur over the whole period of adsorption

It was observed that changes in properties that result in "temporary" increase in temperature at the start of adsorption tends to increase the rate of adsorption, while changes that result in a "temporary" decrease in temperature at the start of adsorption tends to decrease the rate of adsorption.

CHAPTER 6 CONCLUSION AND RECOMMENDATIONS

6.1 Conclusion

From the work carried out it was observed that the during the adsorption process the temperature of the pellet often rises above that of the fin to which it is attached, but high pellet temperatures are not sustained for a long time as the pellet temperature drops to values close to that of the fin shortly after adsorption commences.

As has been proven by previous research, the equilibrium loading capacity of an adsorbent is a function of the evaporator pressure and adsorbent temperature, while the diffusivity is only a function of the adsorbent temperature. The adsorption kinetics is affected mainly by these two properties, that is; the equilibrium loading capacity and the diffusivity.

Changes in the adsorbent temperature affects these two properties, but while the relationship between temperature and diffusivity is directly proportional, that between adsorbent temperature and loading capacity is inversely proportional. This leads to two opposing effects occurring with temperature change, in which one tends to increase the rate of adsorption while the other tends to reduce it.

It was also observed that there was a weakness in the LDF model at early times. This is because the adsorption process at early times is quite sensitive to higher temperatures which occur at the edge of the pellet therefore driving faster diffusion rates. This sensitivity is attributable to high activation energy E_a in $D_s = D_{so}\exp(-E_a/RT)$ where D_s is the surface diffusivity[25].

In summary, from the simulations carried out the following inferences can be drawn

1) Changes in temperature results in opposing effects on the rate of adsorption, these effects are expressed in the form of equilibrium loading capacity and diffusivity
2) At the start of adsorption, when the LDF model is used, the effect of equilibrium loading capacity dominates, thereby resulting in a slower rate of adsorption as temperature increases. Whereas, in the diffusion model, the effect of diffusivity dominates, resulting in faster rate of adsorption as temperature increases.
3) Simply reducing the temperature of adsorption does not necessarily result in a faster adsorption rate, the temperature gradients as well as the temperature history of the process should also be taken into account. Where and when the temperature changes occur is also important.
4) Properties that result in high temperature gradients at the start of adsorption could be beneficial if the adsorption stage of the refrigeration cycle would be cut off shortly after this period, or if the increase in temperature is temporary, i.e. if the increase in temperature is not sustained for a long time.

6.2 Recommendations for Further Work

Further work on this research can be carried out in the following areas:

The effect of loading on the thermal conductivity of the pellet was discussed in section 2.9, in this research the thermal conductivity was set to be constant in a bid to simplify the models, by reducing the degree of non-linearity present. For further work the effect of varying thermal conductivity can be directly coupled, in this case the thermal conductivity of the pellet would be determined by the current loading of the pellet and not set as a constant value. This would give a more detailed and better simulation of the adsorption process.

The effect of varying density can also be studied, in a similar way, where the density of the pellet is also determined by the current loading of the pellet.

REFERENCES/BIBLIOGRAPHY

1. Ahamat, M.A. and M.J. Tierney, *Calorimetric assessment of adsorbents bonded to metal surfaces: Application to type A silica gel bonded to aluminium.* Applied Thermal Engineering (Submitted), 2011.
2. Kim, D.S. and C.A. Infante Ferreira, *Solar refrigeration options - a state-of-the-art review.* International Journal of Refrigeration, 2008. **31**(1): p. 3-15.
3. Wang, D.C., et al., *A review on adsorption refrigeration technology and adsorption deterioration in physical adsorption systems.* Renewable and Sustainable Energy Reviews, 2010. **14**(1): p. 344-353.
4. Zhai, X.Q., et al., *Design and performance of a solar-powered air-conditioning system in a green building.* Applied Energy, 2008. **85**(5): p. 297-311.
5. Zhai, X.Q., et al., *Solar integrated energy system for a green building.* Energy and Buildings, 2007. **39**(8): p. 985-993.
6. Wang, D.C., et al., *Study of a novel silica gel-water adsorption chiller. Part II. Experimental study.* International Journal of Refrigeration, 2005. **28**(7): p. 1084-1091.
7. Critoph, R.E., *Activated carbon adsorption cycles for refrigeration and heat pumping.* Carbon, 1989. **27**(1): p. 63-70.
8. Wang, R.Z. and R.G. Oliveira, *Adsorption refrigeration--An efficient way to make good use of waste heat and solar energy.* Progress in Energy and Combustion Science, 2006. **32**(4): p. 424-458.
9. Thomas, W.J. and B. Crittenden, *Adsorption Technology and Design*. 1998: Elsevier Science and Technology Books.
10. Do, D.D., *Adsorption Analysis: Equillibria and Kinetics*. Series on Chemical Engineering. Vol. 2. 1998: Imperial College Press.
11. Yang, R.T., *Adsorbents: Fundamentals and Applications*. 2003: Wiley Interscience.
12. Suzuki, M., *Adsorption Engineering*. 1990: Elsevier.
13. Srivastava, N.C. and I.W. Eames, *A review of adsorbents and adsorbates in solid-vapour adsorption heat pump systems.* Applied Thermal Engineering, 1998. **18**(9-10): p. 707-714.
14. Wang, L.W., R.Z. Wang, and R.G. Oliveira, *A review on adsorption working pairs for refrigeration.* Renewable and Sustainable Energy Reviews, 2009. **13**(3): p. 518-534.
15. Jakob, D.U. and W. Mittelbach, *Development and investigation of a compact silica gel/water adsorption chiller integrated in solar cooling systems*, in *VII Minsk International seminar*. 2008: Minsk, Belarus.
16. Cornford, J., et al., *Low cost solar coolers for food refrigeration in the developing world*, in *Department of Mechanical Engineering*. 2010, University of Bristol: Bristol.
17. Muris, G., et al., *Demonstration of the honigmann cycle as a method of thermal energy storage*, in *Mechanical Engineering*. 2011, University of Bristol: Bristol.
18. Farooq, S. and D.M. Ruthven, *A comparison of linear driving force and pore diffusion models for a pressure swing adsorption bulk separation process.* Chemical Engineering Science, 1990. **45**(1): p. 107-115.
19. El-Sharkawy, I.I., *On the linear driving force approximation for adsorption cooling applications.* International Journal of Refrigeration, 2011. **34**(3): p. 667-673.
20. Raymond, A. and S. Garimella, *Intraparticle Mass Transfer in Adsorption Heat Pumps: Limitations of the Linear Driving Force Approximation.* Journal of Heat Transfer, 2011. **133**(4): p. 042001-13.
21. Chua, H.T., et al., *Transient modeling of a two-bed silica gel-water adsorption chiller.* International Journal of Heat and Mass Transfer, 2004. **47**(4): p. 659-669.
22. Montastruc, L., et al., *Kinetic Modeling of Isothermal or Non-isothermal Adsorption in a Pellet: Application to Adsorption Heat Pumps.* Chinese Journal of Chemical Engineering, 2010. **18**(4): p. 544-553.

23. Glueckauf, E., *Theory of chromatography. Part 10.-Formulae for diffusion into spheres and their application to chromatography.* Transactions of the Faraday Society, 1955. **51**: p. 1540-1551.
24. Sircar, S. and J.R. Hufton, *Why Does the Linear Driving Force Model for Adsorption Kinetics Work?* Adsorption, 2000. **6**(2): p. 137-147-147.
25. Tierney, M.J., *Discussions on MSc thesis of author*, A.O. Dada, Editor. 2011: Bristol.
26. Pesaran, A.A. and A.F. Mills, *Moisture transport in silica gel packed beds--I.Theoretical study.* International Journal of Heat and Mass Transfer, 1987. **30**(6): p. 1037-1049.
27. Pesaran, A.A. and A.F. Mills, *Moisture transport in silica gel packed beds--II. Experimental study.* International Journal of Heat and Mass Transfer, 1987. **30**(6): p. 1051-1060.
28. Gurgel, J.M. and R.P. Klüppel, *Thermal conductivity of hydrated silica-gel.* The Chemical Engineering Journal and the Biochemical Engineering Journal, 1996. **61**(2): p. 133-138.
29. Tanashev, Y. and Y. Aristov, *Thermal conductivity of a silica gel + calcium chloride system: The effect of adsorbed water.* Journal of Engineering Physics and Thermophysics, 2000. **73**(5): p. 876-883-883.
30. Carson, J.K., et al., *An analysis of the influence of material structure on the effective thermal conductivity of theoretical porous materials using finite element simulations.* International Journal of Refrigeration, 2003. **26**(8): p. 873-880.
31. Tierney, M.J., *2-Dimensional Finite Elements Java Routines*. 2010, Tierney, M.J: Bristol.
32. Tierney, M.J., *2-dimensional representation of pellet problem*, A.O. Dada, Editor. 2011: Bristol.
33. Mathworks, I., *Matlab R2010a Documentation*. 2010.
34. Lewis, R.W., P. Nithiarasu, and K.N. Seetharamu, *Fundamentals of the Finite Element Method for Heat and Fluid Flow*. 2004: John Wiley & Sons, Ltd.
35. Clarkson, C.R. and R.M. Bustin, *The effect of pore structure and gas pressure upon the transport properties of coal: a laboratory and modeling study. 2. Adsorption rate modeling.* Fuel, 1999. **78**(11): p. 1345-1362.